Novel role of GPR109A in thymic regulatory T cell development

Laurence Macia (laurence.macia@sydney.edu.au)
The University of Sydney https://orcid.org/0000-0003-0835-851X
Duan Ni
University of Sydney https://orcid.org/0000-0002-3902-2843
Jian Tan
The University of Sydney
Remy Robert
Monash University
Jemma Taitz
The University of Sydney https://orcid.org/0000-0003-2224-9088
Anjie Ge
The University of Sydney
Camille Potier-Villette
The University of Sydney
Julen Reyes
The University of Sydney
Alanna Spiteri
Charles Perkins Centre, University of Sydney
Claire Wishart
Charles Perkins Centre, University of Sydney
Charles Mackay
Monash University
Laura Piccio
The University of Sydney
Nicholas King
Charles Perkins Centre, University of Sydney https://orcid.org/0000-0002-3877-9772

Article

Keywords: GPR109A, regulatory T cell (Treg), Treg development, thymic medullary epithelial cell (mTEC), experimental autoimmune encephalomyelitis (EAE)

Posted Date: February 23rd, 2023

DOI: https://doi.org/10.21203/rs.3.rs-2609653/v1

Additional Declarations: (Not answered)

Title

Novel role of GPR109A in thymic regulatory T cell development

Duan Ni[1,2], Jian Tan[1,2], Remy Robert[3], Jemma Taitz[1,2], Anjie Ge[1,2], Camille Potier-Villette[1,2], Julen Gabirel Araneta Reyes[1,2], Alanna Spiteri[1,2,4], Claire Wishart[1,2,4], Charles Mackay[3], Laura Piccio[5,6], Nicholas Jonathan Cole King[1,2,4], Laurence Macia[1,2,7]

[1] Charles Perkins Centre, The University of Sydney, Sydney, NSW, Australia

[2] School of Medical Sciences, Faculty of Medicine and Health, The University of Sydney, Sydney, NSW, Australia

[3] Department of physiology, Biomedicine Discovery Institute, Monash University, Clayton, Victoria, Australia

[4] Viral Immunopathology Laboratory, Infection, Immunity and Inflammation Research Theme, School of Medical Sciences, Faculty of Medicine and Health, The University of Sydney, Sydney, NSW, Australia

[5] Brain and Mind Centre and Charles Perkins Centre, School of Medical Sciences, University of Sydney, Sydney, 2050, NSW, Australia

[6] Department of Neurology, Washington University School of Medicine, St. Louis, MO, United States

[7] Sydney Cytometry, The University of Sydney and Centenary Institute, Sydney, NSW, Australia

Correspondence:
Laurence Macia
laurence.macia@sydney.edu.au

Running title

GPR109A suppresses thymic Treg development

Keywords:

GPR109A, regulatory T cell (Treg), Treg development, thymic medullary epithelial cell (mTEC), experimental autoimmune encephalomyelitis (EAE)

Abstract

Regulatory T cells (Treg) maintain immune homeostasis due to their anti-inflammatory functions. They can be generated either centrally in the thymus or in peripheral organs. Metabolites such as short chain fatty acids produced by intestinal microbiota can induce peripheral Treg differentiation, by activating G-protein-coupled-receptors like GPR109A. In this study, we identified a novel role for GPR109A on thymic Treg development. We found that *Gpr109a*$^{-/-}$ mice had increased Treg under basal conditions in multiple organs compared to wild type mice (WT). GPR109A was not expressed on T cells but on medullary thymic epithelial cells (mTECs), as revealed by single cell RNA sequencing in both mice and humans and confirmed by flow cytometry in mice. mTECs isolated from *Gpr109a*$^{-/-}$ mice had higher expression of autoimmune regulator (AIRE), the key regulator of Treg development, while the subset of mTECs that did not express *Gpr109a* displayed increased *Aire* expression and enhanced signalling related to mTEC functionality as well. Increased thymic Treg in *Gpr109a*$^{-/-}$ mice was associated with protection from experimental autoimmune encephalomyelitis, with ameliorated clinical signs and reduced inflammation.

This work identifies a novel role for GPR109A and by extension, the gut microbiota, on thymic Treg development via its regulation of mTECs.

Introduction

Breakdown of immune tolerance results in disease development, including autoimmune and allergic diseases. Regulatory T cells (Treg) are a subset of anti-inflammatory T cells considered to be a central player in immune tolerance with their ability to control the immune response and restore homeostasis. Reduction in the number and function of Treg has been reported in a wide range of chronic inflammatory diseases, including obesity, allergies and autoimmune diseases (1-3), while adoptive transfer of Treg has been shown to have therapeutic potential in inflammatory diseases (4), including graft-versus-host disease (5, 6), refractory ulcerative colitis (7) and multiple sclerosis (8).

Treg have two origins. They either develop centrally in the thymus during thymopoiesis, or in the periphery from naïve T cells in response to environmental cues (9-11). Discrimination of these populations is based on the expression of the transcription factor, Helios, with thymic-derived Treg (tTreg) identified as $CD3^+CD4^+CD25^+FoxP3^+Helios^+$ and peripherally induced Treg (pTreg) as $CD3^+CD4^+CD25^+FoxP3^+Helios^-$ (12). tTreg differentiation is mainly orchestrated by mTECs through TCR-MHCII interaction, CD28 co-stimulation and cytokine signals, such as IL-2, and IL-15 (13, 14). mTEC are uniquely able to present a myriad of tissue-restricted antigens (TRAs), the expression of which is regulated by the transcription factor, autoimmune regulator (AIRE). *Aire*-deficient mice have reduced TRA expression (15-18), which alters the Treg TCR repertoire and functionality, impairs tTreg generation and leads to the spontaneous development of autoimmune disorders, highlighting the key role of AIRE in inducing central tolerance (19-22). Similarly, *AIRE* mutations in humans are linked to autoimmunity. TRA expression by mTECs is also controlled by the transcription factor Fez family zinc finger protein 2 (FEZF2), which modulates TRAs distinct from those controlled by AIRE (23). $Fezf2^{-/-}$ mice have reduced tTreg generation with an altered

TCR repertoire. They develop autoimmune disorders different from those observed in *Aire*$^{-/-}$ mice (23). pTreg are induced in the periphery from naïve T cells in response to environmental cues, including cytokines and gut microbiota-derived metabolites (24). The gastrointestinal tract is a major site for the generation of pTreg, particularly the colon, where 80% of the Treg are peripherally induced (25). Gut microbiota-derived metabolites, particularly short-chain fatty acids, are key inducers of pTreg (26, 27), through multiple mechanisms, including G-protein-coupled-receptor (GPCR) activation, histone deacetylase inhibition, epigenetic modification and metabolic changes (28-30). GPR109A, a microbial metabolite sensing GPCR, is expressed on myeloid cells. The activation of GPR109A by bacterially-derived SCFA butyrate and niacin has been shown to induce gut-derived Treg through effects on CD103^{+} dendritic cells (31) and colonic macrophages (32), respectively. Mice deficient for GPR109A have a reduced number of Treg in the gastrointestinal tract and are more prone to develop colonic inflammation, carcinogenesis and food allergy (31-33). These results show the critical role of GPR109A in peripheral tolerance, but its role in central tolerance remains unclear.

By studying the immune profile of *Gpr109a* knockout (*Gpr109a*$^{-/-}$) mice, we show for the first time the dual role of GPR109A on thymic *versus* peripheral Treg generation. *Gpr109a*$^{-/-}$ mice had decreased numbers of microbiota-induced Treg, while their tTreg were increased. We identified by flow cytometry that this receptor was not expressed on thymic DP, DN and naïve T cells, which excludes a direct effect, but instead was expressed by mTECs. The absence of GPR109A in the *Gpr109a*$^{-/-}$ mice led to higher AIRE expression, which is aligned with their increased tTreg generation. Furthermore, *Gpr109a*$^{-/-}$ mice were protected from experimental autoimmune encephalomyelitis (EAE), a mouse model of multiple sclerosis, confirming an enhanced tolerance in these mice.

This work reveals a novel mechanism driving the generation of tTreg and the regulation of central tolerance by the gut microbiota. It also highlights the complex impact of gut microbiota on host immunity that needs to be considered when developing interventions targeting gut microbiota to treat diseases.

Materials and Methods

Mice

C57BL/6 male mice were purchased either from Australian Animal BioResources or Animal Resources Centre and were housed under specific-pathogen-free conditions at the Charles Perkins Centre. *Gpr109a*$^{-/-}$ mice were described before (33). All animal experiments were approved by the University of Sydney Animal Ethics Committee (ID 1737).

Flow cytometry analysis

For peripheral blood mononuclear cells, blood was collected through cardiac puncture upon sacrifice. Two rounds of red blood lysis were carried out using 1x red blood cell (RBC) lysis buffer (BioLegend), and then samples were resuspended in fluorescence-activated cell sorting (FACS) buffer (2% FBS containing 1mM ethylenediaminetetraacetic acid (EDTA)).

For spleen, thymus and lymph nodes, organs were mechanically disrupted to prepare a single-cell suspension, followed by filtering through 100µm cell strainers. Red blood cell lysis was carried out using 1x RBC lysis buffer (BioLegend), and then samples were resuspended in FACS buffer.

For central nervous system (CNS), brains and spinal cords were mechanically disrupted to prepare a single-cell suspension, followed by filtering through 100µm cell strainers. The suspension was then centrifuged at 300 x g for 10 minutes at 4 °C to pellet the cells, which further undergo 30%/37%/70% Percoll gradient centrifugation at 1200 x g for 20 minutes at 4 °C without the brake for isolation/enrichment. After isolation and washing, cells were resuspended in FACS buffer until further processing.

For colonic lamina propria leukocyte isolation, organs were processed using a previously established protocol (34). In brief, colons were washed in PBS and then cut into small pieces and incubated in Hanks' Balanced Salt Solution (HBSS) containing 5% FBS, 15mM (4-(2-hydroxyethyl)-1-piperazineethanesulfonic acid) (HEPES), 5mM EDTA, and 100U/ml penicillin-streptomycin (Sigma) to remove epithelial cells. Then, the whole tissues were digested with 6.7mg/ml Collagenase type IV (GIBCO) in HBSS with 10% FBS, 15mM HEPES and 100U/ml penicillin-streptomycin (Sigma). After that, the cell suspension was vortexed and then filtered and isolated with a 40% and 80% Percoll gradient. Cells harvested from the middle ring of the Percoll gradient were then washed before proceeding to further processing.

For thymic epithelial cell isolation, after dissections, thymuses were processed, based on published protocols with modifications (35, 36). In brief, small incisions were first cut in the thymic lobes. The thymus was then placed in RPMI-1640 (GIBCO) supplemented with 2% FBS and pipetted gently to release thymocytes within. After this, the thymus was digested with 0.125% collagenase type IV (GIBCO) in RPMI-1640 for 40-60 minutes at 200 rpm, 37 °C. After digestion, FACS buffer was added to the resulting cell suspension, which was filtered before proceeding to further processing.

For cytokine measurement, cells were cultured in complete RPMI media with phorbol 12-myristate 13-acetate (PMA), ionomycin and brefeldin A for 4 hours in 5% CO_2 at 37 °C, followed by intracellular staining.

For intracellular staining, cells were permeabilized, fixed and stained with the Foxp3/Transcription Factor Staining Buffer kit (eBioscience) according to the manufacturer's protocol.

Antibodies used in experiments are indicated in Table 1. Data was recorded with a BD LSR-II analyser (Becton Dickinson, San Jose, CA, USA) using the FACSDiva software, and were further analyzed with FlowJo v10.8.1. (Treestar Inc. Ashland, OR, USA), with the gating strategies shown in supplementary Fig. S1-S6.

Generation of anti-mouse GPR109A monoclonal antibodies

The anti-mouse GPR109A clone (2D4-B7) was generated and validated as previously described (37). Briefly, *Gpr109a*$^{-/-}$ mice were immunized with 10^7 L1.2 mouse GPR109A transfected cells, intraperitoneally, 6 times at 2-week intervals. The final immunization was injected intravenously. Four days later, the spleen was removed, and cells were fused with the SP2/0 cell line [1581; American Type Cell Collection (ATCC) Cell Lines]. The clone 2D4-B7's specificity toward mouse GPR109A was validated by flow cytometry using transfected cells as well as mature blood neutrophils isolated from WT and *Gpr109a*$^{-/-}$ C57/BL6 mice. Purified clone 6.3 (mouse IgG2c; Southern Biotech) was used in all experiments as isotype control.

Induction and assessment of experimental autoimmune encephalomyelitis (EAE)

For EAE induction, mice were subcutaneously injected with 50µg/mouse myelin oligodendrocyte glycoprotein (MOG_{35-55}: MEV GWY RSP FSRVVH LYR NGK; GenScript) emulsified in incomplete Freund's adjuvant (Chondrex, Inc.) complemented with 50µg desiccated *Mycobacterium tuberculosis* (strain H37RA). Upon immunization and 2-day post immunization, mice were also intravenously injected with 300ng/mouse pertussis toxin (List Biological Laboratories).

Post-immunization, mice were monitored for their clinical signs, based on the criteria shown in Table 2. Clinical courses were evaluated for at least 30 days after immunization and the EAE experiments were repeated at least three times.

Ex vivo proliferation assay and cytokine measurement

For *ex vivo* MOG-specific T cell proliferation assays in EAE experiments, a single-cell suspension was prepared from spleen or lymph nodes from EAE mice at the indicated time points and then labelled with carboxyfluorescein succinimidyl ester (CFSE). Next, cells were cultured in triplicate in 200µl complete RPMI media with the indicated concentration of MOG at 2×10^5 cells per well in 96-well plates for 72 hours in 5% CO_2 at 37 °C. After culture, cells were washed with cold PBS and processed for flow cytometry analysis. Proliferation index was calculated as previously described (38). Quantification of IL-17 cytokine production was carried out by enzyme-linked immunosorbent assay (ELISA) with anti-mouse IL-17 antibody following the manufacturer's protocol.

Histological analysis

After sacrifice, mice were perfused with ice cold 4% paraformaldehyde, and the CNS tissues were fixed in 4% paraformaldehyde for 24 hours. Tissues were then washed with PBS twice and then decalcified with 0.5M EDTA (Sigma Aldrich) for 1 week. During decalcification, the EDTA buffer was changed every 2 days and samples were kept rocking at room temperature. After 1-week of decalcification, tissues were first washed with PBS for 1 hour and then sequentially dehydrated with 30% and 50% ethanol for 30 minutes respectively. Finally, samples were stored in 70% ethanol until further processing.

Histology sections were prepared using standard protocols (39). In brief, tissues were embedded in paraffin and 4μm sections were prepared before being stained with hematoxylin and eosin (H&E). Slides were examined with a light microscope (Zeiss Axioscope) and scored for inflammation by three independent blinded observers, based on the guidelines described in (40) (Table 3).

Analysis of RNA-sequencing and single cell RNA-sequencing data

For RNA-sequencing (RNA-seq) analysis, processed data was extracted from Haemosphere (41-43) and re-analyzed with PRISM GraphPad. For single cell RNA-sequencing (scRNA-seq) analysis, data was downloaded from Gene Expression Omnibus data from previous studies (GEO: GSE131339 and GSE147520) and processed and normalized based on the original paper (44, 45). After that, the data was analyzed and visualized with Seurat 4.1.0. (46-48). Differentially expressed genes comparing *Gpr109a*$^{+}$ and *Gpr109a*$^{-}$ mTECs were analyzed with Seurat's FindMarkers function based on the "DESeq2" method (49) with default settings and the thresholds for differentially genes were defined as $p < 0.05$ and LOG2(Fold Change) values higher than 0.5 or lower than -0.5. GSEA was carried out with FGSEA package (50, 51). Gene scores were generated using Seurat CellCycleScoring function based on the AIRE-dependent TRA gene list described in (52).

Statistics

Data were statistically analyzed with PRISM GraphPad. An unpaired t-test was used when comparing two groups, and two-way ANOVA was used to analyze the EAE clinical curves.

Results

Absence of GPR109A decreased microbiota induced Treg and increased thymic Treg

GPR109A signalling has been shown to have anti-inflammatory effects, with GPR109A deficiency leading to aggravated colitis and food allergy (31, 33). Part of these anti-inflammatory effects are explained by the induction of pTreg in the colon (31, 32). Whether the effect of GPR109A on Treg is limited to the gut or extends to other sites is unknown. To address this question, we evaluated Treg from wild-type (WT) and *Gpr109a* gene knock-out (*Gpr109a*$^{-/-}$) mice by flow cytometry. While the proportion and number of splenic CD4^{+} and CD8^{+} T cells were similar between these mice (Fig. 1A, B, and Supplementary Fig. S7A, B), surprisingly, values for splenic Treg were slightly but significantly increased in *Gpr109a*$^{-/-}$ mice (Fig. 1C, D and Supplementary Fig. S7C). Similarly, *Gpr109a*$^{-/-}$ mice had significantly more Treg in the mesenteric lymph nodes (mLNs) and this effect was more striking in the colon (Fig. 1E-H and Supplementary Fig. S7D, E).

Treg can be generated centrally in the thymus or peripherally. As the gut microbiota has been shown to modulate the T cell compartment in the thymus (53), we investigated whether the absence of GPR109A supported the development of pTreg or tTreg derived Treg. To discriminate the origin of these Treg, we used Helios, a marker for tTreg (12). We observed an increased proportion and number of Helios^{+} tTreg in the spleen of *Gpr109a*$^{-/-}$ mice (Fig. 1 I-J and Supplementary Fig. S7F), suggesting a regulatory role for GPR109A signalling in tTreg generation. RORγt is a marker of pTreg induced by the gut microbiota in the gastrointestinal tract (54). We found that *Gpr109a*$^{-/-}$ mice had a decreased proportion of microbiota-induced RORγt^{+} Treg in the mLN and the colon (Fig. 1 K-N), which is consistent with the absence of microbiota-derived metabolite signalling through this receptor. Similarly, this population was decreased in the spleen (Supplementary Fig.

S7G). Together, these results show that absence of GPR109A signalling favours tTreg development while impairing microbiota-induced pTreg generation.

GPR109A specifically affects thymic Treg development but not thymopoiesis

As tTreg generation occurs during thymopoiesis, we next aimed to determine whether GPR109A affected this process.

During thymopoiesis, progenitors differentiate into DN subsets expressing neither CD4 nor CD8, which further differentiate into DP cells, committing to $CD4^+$ or $CD8^+$ SP T cells. During the negative selection process, $CD4^+$ SP cells undergo apoptosis, or differentiate into naïve T cells (Tn) or Treg (55) (Fig. 2A). By comparing *Gpr109a*$^{-/-}$ and WT mice, we found that the proportion and number of most thymocyte subsets were similar, indicating that GPR109A minimally influenced thymopoiesis (Fig. 2B-E and Supplementary Fig. S8A, B). However, the absence of GPR109A led to higher Treg generation in the thymus (Fig. 2F-G and Supplementary Fig. S8C). This result is consistent with the finding that Helios$^+$ Treg were increased in the periphery in *Gpr109a*$^{-/-}$ mice (Fig. 1).

Taken together, these data indicate that absence of GPR109A supports tTreg development without impacting overall thymopoiesis.

GPR109A indirectly affects thymic Treg generation

To further understand the mechanism behind the effect of GPR109A on tTreg development, we assessed the expression of GPR109A on T lymphocytes in the thymus, spleen and mLN by flow cytometry. We used a monoclonal mouse anti-GPR109A antibody, previously described in (37), that labelled circulating neutrophils, known to express GPR109A. As expected, there was no positive staining in the *Gpr109a*$^{-/-}$ neutrophils (Fig. 3A, B). We next investigated whether

GPR109A was present in different T cells subsets and did not detect its expression in neither Treg, naïve T cells and other T cell subsets in the spleen, thymus and mLN (Fig. 3C and Supplementary Fig. S9A-C). This was further confirmed by our analysis of publicly available RNA-seq data retrieved from Haemosphere (41-43), in which *Gpr109a* transcripts were undetectable in T cells, while present in myeloid cells (Supplementary Fig. S9D).

Taken together, these results show the absence of GPR109A on T cells, suggesting an indirect effect of GPR109A on tTreg generation.

The presence of GPR109A on medullary thymic epithelial cells correlates with reduced AIRE expression

Medullary thymic epithelial cells (mTECs) are key cells in tTreg development through their presentation of a wide range of TRAs (56). By flow cytometry, we identified the presence of GPR109A specifically on mTEC and not on cTEC (Fig. 3D, E), which was also consistent with the RNA-seq analysis from Haemosphere (Supplementary Fig. S9D). Interestingly, a subset of only 15% of mTECs expressed GPR109A (Fig. 3E). mTECs have the particularity of expressing the transcription factor AIRE, which induces the expression of TRAs and promotes Treg generation (56). To determine whether the presence of GPR109A correlated with changes in AIRE expression, we assessed the expression of AIRE in GPR109A^{+} or GPR109A^{-} mTECs from WT mice by flow cytometry. We found that GPR109A^{-} mTECs expressed significantly more AIRE than GPR109A^{+} mTECs (Fig. 3F). The expression of AIRE was also significantly higher in mTECs isolated from *Gpr109a*$^{-/-}$ mice, compared to WT mice (Fig. 3G and Supplementary Fig. S10B).

Altogether our data show that the expression of GPR109A was associated with lower expression of AIRE expression.

The presence of *Gpr109a* in mouse mTECs is associated with changes in properties and reduced tissue-restricted antigen expression

To decipher the potential role of GPR109A on mTEC function, we analysed previously published single cell RNA sequencing (scRNA-seq) data of TECs (44). A total of 2093 cells were extracted for downstream analysis after standardized data pre-processing and normalization as described in the original study. Single cells were next projected into a two-dimensional space using Uniform Manifold Approximation and Projection (UMAP). As shown in Figure 5A, TECs were clustered into mTECs (1651 cells) and cTECs (442 cells). We found that *Gpr109a* was preferentially expressed in mTECs (Fig. 4A), consistent with our flow cytometry data (Fig. 3E).

Next, mTEC populations were subsetted into *Gpr109a*$^-$ mTECs and *Gpr109a*$^+$ mTECs, based on their zero or superior *Gpr109a* expression levels, respectively, and comparative analyses on these two subsets were carried out to investigate the potential role of GPR109A and its downstream signalling in mTECs. Differential gene expression analysis with DESeq2 (49) revealed that 48 genes were up-regulated and 35 down-regulated in *Gpr109a*$^-$ mTECs, compared to *Gpr109a*$^+$ mTECs (Fig. 4B). *Aire* and *Fezf2*, two critical transcription factors promoting the expression of TRAs and thus of Treg generation (27, 56), were significantly up-regulated in *Gpr109a*$^-$ mTECs (Fig. 4C, D). Importantly, the gene set score for AIRE-dependent TRA genes (52) was also significantly higher in *Gpr109a*$^-$ mTECs (Fig. 4E). Interestingly, in comparing *Gpr109a*$^-$ mTECs with *Gpr109a*$^+$ mTECs, TRA genes corresponding to various tissues were differentially expressed. For example, TRA gene set scores for CNS and thymus were increased in *Gpr109a*$^-$ mTECs, while those for hair and liver were decreased (Supplementary Fig. 11A).

To further interrogate the impact of GPR109A on the intracellular signalling pathways within mTECs, Gene Set Enrichment Analysis (GSEA) was carried out comparing *Gpr109a*$^{-}$ and *Gpr109a*$^{+}$ mTECs. This revealed that *Gpr109a*$^{-}$ mTECs were enriched in gene sets involved in Myc- and ribosome-related signalling pathways (Fig 4F, G and Supplementary Fig. 11B, C), both of which were associated with the control of mTEC transcriptional program and functionality (44, 52).

Altogether, the expression of *Gpr109a* in mTECs correlates with changes in the expression of genes modulating their properties and functions, which are related to tTreg induction.

The presence of *GPR109A* on human mTECs is associated with changes in *AIRE* and *FEZF2* expression and ribosomal signalling

To determine whether these effects were also observed in humans, we analysed published scRNA-seq data from human thymic stromal cells (45). Analysis was done on 14,217 cells isolated at different stages of life, from fetal (19 and 23 weeks), to postnatal (6 days and 10 months), and adulthood (25 years old) (Fig. 5A, B), in which the expression of *GPR109A* was consistently detected (Fig. 5C). As observed in mice, we found that *GPR109A* was predominantly expressed in mTECs and not in cTECs. Notably, the expression of *GPR109A* was also detected in a group of immature TECs, which were only present in adult human thymus (Fig. 5C). Comparative analysis found that *GPR109A*$^{-}$ mTECs exhibited higher *AIRE* and *FEZF2* expression relative to *GPR109A*$^{+}$ mTECs (Fig. 5D, E), consistent with the findings in mouse mTECs. Human *GPR109A*$^{-}$ mTECs also showed enrichment in gene expression linked to ribosomal pathway (Fig. 5F).

Lack of GPR109A signalling in *Gpr109a*$^{-/-}$ mice reduces EAE severity

Treg play an important role in the control of the immune response (57, 58), with autoimmune diseases commonly linked to defects in the Treg population (1, 2). Multiple sclerosis (MS) is a demyelinating autoimmune disease characterised by an imbalance in the Treg:Th17-Th1 ratio (59). Rescuing the Treg population has promising effects in the clinic, with decreased disease relapses in MS patients (8, 60). Experimental autoimmune encephalomyelitis (EAE) is a mouse model of MS in which Treg, particularly tTreg, are critical for control of the disease symptoms (61) and their depletion exacerbates disease severity (62). To determine whether increased Treg generated in *Gpr109a*$^{-/-}$ mice were functional, we immunised WT versus *Gpr109a*$^{-/-}$ mice with MOG_{35-55} to induce EAE, as previously described (38, 39) (Fig. 6A). The incidence of disease was similar in both groups, with onset of disease appearing around day 10 in each (Fig.6A, B and Supplementary Fig. S12A, B). However, the severity of disease was significantly decreased in the *Gpr109a*$^{-/-}$ group, as reflected by their reduced overall clinical scores and the associated areas under curve (AUC) (Fig. 6B and Supplementary Fig. S12C-F, S13). Inflammation and demyelination were analyzed in the spinal cords of EAE mice. Histological analysis showed that *Gpr109a*$^{-/-}$ mice showed significantly reduced neuroinflammation and leukocyte infiltration and milder demyelination (Fig. 6C, D and Supplementary Fig. 12G), consistent with their clinical signs.

The neuroinflammation and demyelination during EAE is due to the infiltration of leukocytes, particularly the monocyte influx, and their further differentiation into macrophages, as well as the activation of microglia. Flow cytometric analysis of the CNS from EAE animals on day 36 revealed that compared with WT mice, *Gpr109a*$^{-/-}$ mice exhibited a significantly decreased proportion of inflammatory myeloid cells in their CNS (Fig. 6E, F). Notably, in both the CNS and the spleen, *Gpr109a*$^{-/-}$ mice had larger fractions of Treg, and their numbers were also significantly increased in these organs as well (Fig. 6G-J, Supplementary Fig. 14). This was accompanied by

reduced MOG antigen-specific responses in draining lymph nodes, including antigen-specific T cell proliferation and IL-17 production at day 7 post-immunization (Supplementary Fig. 15). Together, these results show that *Gpr109a*$^{-/-}$ mice had increased Treg and were protected against CNS autoimmunity.

Discussion

Treg play a key role in immune tolerance and homeostasis. Among the environmental factors supporting peripheral tolerance, gut microbiota-derived metabolites have a well-reported role in the development of pTreg. The present work highlights a novel role for the gut microbiota in central tolerance, with an inhibitory effect of bacterial metabolite receptor signalling on tTreg development. We identified the presence of the niacin and butyrate receptor, GPR109A, in mTECs, key cells supporting tTreg development. Expression of GPR109A in mTECs was associated with less AIRE expression, while the absence of GPR109A in knockout mice led to higher proportion of AIRE-expressing mTECs and increased tTreg generation. This translated into less severe EAE pathology. This work gives novel insight into the impact of gut bacteria on immune homeostasis.

Previous studies have shown that GPR109A signalling induced pTreg generation either via $CD103^+$ DC or colonic macrophages (31, 32). We show in the present work that GPR109A signalling also modulated tTreg generation via indirect effects on mTECs. GPR109A was not expressed on naïve T cells, consistent with a previous report by Docampo *et al* (63). In contrast to pTreg generation, increased numbers of tTreg were induced in the absence of GPR109A signalling. Absence of GPR109A in knockout mice was associated with increased expression of *Aire*, a key transcription factor supporting tTreg generation. We identified subsets of mTECs that expressed *Gpr109a*, both in mice and humans by scRNA-seq analyses and in mice at the protein level by flow cytometry. The *Gpr109a*$^-$ subset of mTECs expressed higher levels of *Aire* and *Fezf2,* suggesting a negative role for GPR109A on these key Treg-inducing transcription factors.

The impact of GPCR ligands like SCFA on AIRE expression has already been reported in the thymus of offspring mice from germ-free mice treated with acetate (64) or fed on a high fibre diet

during pregnancy (65). The former study showed that acetate increased AIRE expression in cTECs but not mTECs, which did not increase Treg generation. The latter study showed that butyrate increased tTreg generation in organoids via GPR41, although our scRNA-seq analysis in mouse mTECs suggested very low levels of *Gpr41* expression. The opposing effects of SCFA on the GPCRs, in which GPR41 promotes and GPR109A inhibits tTreg generation may be a preserved mechanism to tightly control tTreg numbers. AIRE and FEZF2 also contribute to Treg TCR repertoire diversity. Whether the absence of GPR109A affects Treg TCR diversity is out of the scope of this study but would be of interest to further understand how gut bacterial products shape host immunity.

GPR109A not only binds SCFA butyrate but also other ligands such as niacin (66) and ketone body β-hydroxybutyric acid (67). A previous study showed that very low levels of serum butyrate were detectable (68), but whether these fluctuate depending on feeding status is unknown. A comprehensive analysis of the mouse multiple-tissue metabolome failed to detect butyrate or niacin in the mouse thymus, while a low level of ketone body β-hydroxybutyric acid could be found (69). Whether β-hydroxybutyric acid is the natural ligand for thymic GPR109A involved in tTreg generation requires further investigation. Like dietary fibre and butyrate, fasting and β-hydroxybutyric acid have been shown to support Treg generation (40, 70), possibly via GPR109A.

mTEC function is dependent on Myc and ribosome-related signalling pathways (44, 52). GSEA revealed that *Gpr109*$^{-}$ mTECs had significantly higher enrichment in these pathways, suggesting that the absence of GPR109A might fine-tune mTEC activity by regulating Myc and ribosome signalling pathways. The activation of GPR109A by butyrate, niacin and dimethyl fumarate was reported to consistently reduce Myc activation (71-73). This is consistent with our observation that *Gpr109*$^{+}$ mTECs had reduced expression of genes involved in the Myc signalling pathway. Further

investigation linking GPR109A and Myc would be needed to clarify the mechanisms behind the effects of GPR109A on tTreg generation.

Notably, by analyzing scRNA-seq data from human thymic stromal cells, we found that *GPR109A* was also predominantly expressed in mTECs. Its expression was associated with reduced levels of *AIRE* and *FEZF2* in human mTECs, as well as compromised ribosomal signalling. This suggested a preserved role for GPR109A in mouse and human mTECs.

We observed that the types of TRA expressed by *Gpr109*$^{+}$ mTECs were different *Gpr109*$^{-}$ mTECs. Epigenetic changes, such as histone acetylation, have been shown to play a critical role in both AIRE-dependent and -independent TRA expression (74), with the histone acetyltransferase, KAT7, and histone deacetylase, HDAC3, regulating AIRE and AIRE-targeted gene expression in mTECs (75). As butyrate signalling through GPR109A has been shown to inhibit HDAC activity, the absence of GPR109A signalling could affect histone acetylation and explain the differential expression of *Aire* and TRA genes in *Gpr109a*-positive and negative mTECs. Importantly, we found an increase in CNS TRA expression in *Gpr109a*$^{-}$ mouse mTECs, which could explain the protection of *Gpr109a*$^{-/-}$ mice from EAE. SCFA have been shown to increase Treg generation with beneficial effects in human MS (76). However, this study focused on the role of propionic acid, which does not signal via GPR109A. Whether blocking GPR109A has benefits in human MS remains unknown. We also observed a decreased expression of TRAs specific for the liver and lymphoid cells in *Gpr109a*$^{-}$ mTECs, but no differences for TRAs of the lungs or kidney. GPR109A signalling may thus regulate immune tolerance towards specific organs.

Targeting GPR109A with agonists has been suggested as a new therapeutic avenue in a broad range of diseases (77, 78). Our work suggests that an organ-specific targeted action may be a better alternative to preserve tTreg generation and reduce the risk of autoimmune disease development.

Acknowledgements

We sincerely thank Professor Jean Yang, Professor Hang Ruan and Professor Youqiong Ye for discussion on bioinformatic analysis, Professor Michael Buckland and Maggie Le for helping with the preparation of the histology slides, the Sydney Cytometry Core Facility for providing access to flow cytometer analysers, and the Laboratory Animal Services of the University of Sydney for animal housing and husbandry. Part of the components of figures were created with Servier Medical Art templates, which are licensed under a Creative Commons Attribution 3.0 Unported Licence: https://smart.servier.com. This project was funded by the Australian Research Council grant APP160100627, and Multiple Sclerosis Research Australia/Incubator Grant 204-0000000057. L.M. and J.T. are a'Beckett fellows. D.N. is a recipient of the Australian Government Research Training Program Scholarship (International).

Author Contributions

D.N. performed most of the experiments, participated in the project design and wrote the manuscript, L.P., J.T., J.Taitz, A.G., C.P-V, and J.G.A.R. participated in the experiments, A.S. and C.W. helped with the data analysis, R.R. and C.M. produced the anti-GPR109A antibody, L.P. and N.J.C.K. helped with the study design, L.M. participated in the experiments, and study design, supervised the study and wrote the manuscript. All authors reviewed and edited the manuscript.

Conflict of Interest

The authors declare no conflict of interest.

Figure Legend

Fig 1. *Gpr109a*$^{-/-}$ mice showed Treg imbalance with increased thymic derived Treg and decreased microbiota-induced Treg.

(**A**-**B**) Proportions of CD4$^+$ and CD8$^+$ T cells in total leukocytes (CD45$^+$) were analyzed by flow cytometry in spleens of wild-type (WT) and *Gpr109a*$^{-/-}$ mice. **A.** Representative flow cytometric plots of spleen CD4$^+$ and CD8$^+$ T cells in WT (left) and *Gpr109a*$^{-/-}$ (right) mice. **B.** Scatter bar chart for the proportions of CD4$^+$ and CD8$^+$ T cells in spleens from WT and *Gpr109a*$^{-/-}$ mice.

(**C**-**H**) Proportions of regulatory T cells (Treg) in total CD4$^+$ T cells of WT (left) and *Gpr109a*$^{-/-}$ (right) mice and their representative flow cytometric plots in spleen (**C**-**D**), mesenteric lymph nodes (mLNs) (**E**-**F**) and colon (**G-H**) respectively.

(**I**-**J**) Proportions of thymic derived (Helios$^+$) Treg among total Treg population in spleens of WT (left) and *Gpr109a*$^{-/-}$ (right) mice. **I.** Representative flow cytometric plots of Helios$^+$ Treg in WT (left) and *Gpr109a*$^{-/-}$ (right) mice. **J.** Scatter bar chart for the proportions of Helios$^+$ Treg in spleens from WT and *Gpr109a*$^{-/-}$ mice.

(**K**-**L**) Proportions of microbiota-induced (RORγt$^+$) Treg among total Treg population in mLNs of WT (left) and *Gpr109a*$^{-/-}$ (right) mice. **K.** Representative flow cytometric plots of RORγt$^+$ Treg in WT (left) and *Gpr109a*$^{-/-}$ (right) mice. **L.** Scatter bar chart for the proportions of RORγt$^+$ Treg in mLNs from WT and *Gpr109a*$^{-/-}$ mice.

(**M**-**N**) Proportions of microbiota-induced (RORγt$^+$) Treg among total Treg population in colon of WT (left) and *Gpr109a*$^{-/-}$ (right) mice. **M.** Representative flow cytometric plots of RORγt$^+$ Treg in WT (left) and *Gpr109a*$^{-/-}$ (right) mice. **N.** Scatter bar chart for the proportions of RORγt$^+$ Treg in colon from WT and *Gpr109a*$^{-/-}$ mice.

N=6-8 per group and data are presented as mean ± s.e.m. with * p<0.05, ** p<0.01, *** p<0.001 by unpaired t-test.

Fig 2. *Gpr109a*$^{-/-}$ mice showed increased thymic Treg generation but not thymopoiesis.

A. An overview of the thymopoiesis process.

(**B**-**C**) Proportions of double-negative (DN), double-positive (DP), CD4$^+$ and CD8$^+$ T cells in total leukocytes (CD45$^+$) were analyzed by flow cytometry in thymus of wild-type (WT) and *Gpr109a*$^{-/-}$ mice. **B.** Representative flow cytometric plots of thymus DN, DP, CD4$^+$ and CD8$^+$ T cells in WT (left) and *Gpr109a*$^{-/-}$ (right) mice. **C.** Scatter dot plots of the proportions of DN, DP, CD4$^+$ and CD8$^+$ T cells in thymus from WT and *Gpr109a*$^{-/-}$ mice.

(**D**-**E**) Proportions of double-negative one to four (DN1-DN4) populations in total DN T cells in thymus of wild-type (WT) and *Gpr109a*$^{-/-}$ mice. **D.** Representative flow cytometric plots of thymus DN1-DN4 populations in WT (left) and *Gpr109a*$^{-/-}$ (right) mice. **E.** Scatter dot plots of the proportions of DN1-DN4 populations in thymus from WT and *Gpr109a*$^{-/-}$ mice.

(**F-G**) Proportions of Treg in total CD4$^+$ T cells in thymus of wild-type (WT) and *Gpr109a*$^{-/-}$ mice. **F.** Representative flow cytometric plots of thymus Treg in WT (left) and *Gpr109a*$^{-/-}$ (right) mice. **G.** Scatter dot plots of the proportions of Treg in thymus from WT and *Gpr109a*$^{-/-}$ mice.

N=6-8 per group and data are presented as mean ± s.e.m. with ** p<0.01 by unpaired t-test.

Fig 3. GPR109A was not expressed in T cells but in thymic medullary epithelial cells (mTECs) and was associated with reduced AIRE expression.

(**A**-**B**) Staining of GPR109A in circulating mouse neutrophils. **A.** Histogram for staining of GPR109A in circulating mouse neutrophils (Ly6G$^+$) in WT (red) and *Gpr109a*$^{-/-}$ (orange) mice and the isotype control for the monoclonal Ab (cyan). **B.** Scatter bar chart for the proportions of GPR109A$^+$ neutrophils in WT and *Gpr109a*$^{-/-}$ mice and the isotype control for the monoclonal Ab.

(**C**) Histograms for staining of GPR109A in splenic naïve CD4$^+$ T cells, splenic Treg and thymic Treg and their corresponding isotype control.

(**D**-**E**) Staining of GPR109A in thymic medullary epithelial cells (mTECs). **D.** Histogram for staining of GPR109A in mTECs in WT (red) and *Gpr109a*$^{-/-}$ (orange) mice and the isotype control for the monoclonal Ab (cyan). **E.** Scatter bar chart for the proportions of GPR109A$^+$ mTECs and cTECs in WT mice and the corresponding isotype control for the monoclonal Ab.

F. Scatter bar chart of the proportions of AIRE$^+$ mTECs from GPR109A$^+$ mTECs versus GPR109A$^-$ mTECs.

G. Scatter bar chart of the proportions of AIRE$^+$ mTECs in WT and *Gpr109a*$^{-/-}$ mice.

N=5-8 per group and data are presented as mean ± s.e.m. with * $p<0.05$, *** $p<0.001$, **** $p<0.0001$ by unpaired t-test.

Fig 4. Single cell RNA-sequencing (scRNA-seq) of mouse thymic epithelial cells identifies *Gpr109a*-expressing mTEC subset, which exhibits reduced mTEC functions and re-wired intracellular signals.

A. *Gpr109a* is expressed predominantly in mTECs but not thymic cortical epithelial cells (cTECs). The uniform manifold approximation and projection (UMAP) visualized mouse mTECs and cTECs from scRNA-seq results. Colored dots denoted cells that expressed *Gpr109a*, and the color density reflected the expression level of *Gpr109a*.

B. Volcano plot showing differentially expressed genes in the comparison of *Gpr109a*$^+$ *and Gpr109a*$^-$ mTECs. The red dots denoted genes up-regulated in *Gpr109a*$^-$ mTECs, the blue dots denoted genes down-regulated in *Gpr109a*$^-$ mTECs, and the black ones are genes without significant changes.

(**C-D**) Violin plots of the expression profiles of *Aire* (**C**) and *Fezf2* (**D**) in *Gpr109a*$^+$ mTECs (red) versus *Gpr109a*$^-$ mTECs (cyan). Red dots indicate the average expression levels of the corresponding groups.

E. Violin plots of the gene module score of AIRE-dependent tissue restricted antigen (TRA) genes in *Gpr109a*$^{+}$ mTECs (red) versus *Gpr109a*$^{-}$ mTECs (cyan). Red dots indicated the average expression levels of the corresponding groups.

(**G-H**) Gene set enrichment analysis (GSEA) showing enrichment of Myc-target signalling and ribosomal signalling pathways in *Gpr109a*$^{+}$ mTECs versus *Gpr109a*$^{-}$ mTECs.

Fig 5. scRNA-seq of human thymic stromal cells identifies *GPR109A*-expressing mTEC subset, which exhibits reduced mTEC functions and re-wired intracellular signals.

A. The UMAP visualized thymic stromal cells colored by age group (fetal 19 weeks, fetal 23 weeks, postnatal 6 days, postnatal 10 months and adult 25 years old).

B. The UMAP visualized thymic stromal cells colored by cell types (immature TEC, cTEC, mTEC, neuroendocrine cell, myoid cell, and myelin^{+} cell).

C. *GPR109A* is expressed predominantly in mTECs and immature TECs but not cTECs. The UMAP visualizes human thymic stroma cells from scRNA-seq results. Colored dots denote cells that expressed *GPR109A*, and the color density reflects the expression level of *GPR109A*.

(**D-E**) Violin plots of the expression profiles of *AIRE* (**D**) and *FEZF2* (**E**) in *GPR109A*$^{+}$ mTECs (red) versus *GPR109A*$^{-}$ mTECs (cyan). Red dots indicate the average expression levels of the corresponding groups.

F. GSEA showing enrichment of ribosomal signalling pathways in *GPR109A*$^{+}$ mTECs versus *GPR109A*$^{-}$ mTECs.

Fig 6. *Gpr109a*$^{-/-}$ mice show attenuated experimental autoimmune encephalomyelitis (EAE) compared with WT mice.

A. Study timeline. WT or *Gpr109a*$^{-/-}$ mice were immunized with myelin oligodendrocyte glycoprotein (MOG) emulsified in incomplete Freund's adjuvant supplemented with heat-killed *M.Tuberculosis* and injected with pertussis toxin at D0, and 2 days later animals received second

injection of pertussis toxin. On D7, 3 mice from each group were sacrificed and their draining lymph nodes were dissected and used for an *ex vivo* MOG-specific proliferation assay. The remaining 8 mice from each group were kept and monitored for clinical signs until culled on D36 as the final endpoint. Total mouse number for study, disease incidence and disease-related mortality are reported in the table.

B. EAE clinical course of sick mice during EAE comparing WT (filled dots) and *Gpr109a*$^{-/-}$ (hollow dots) mice (n=6-7 per group).

C. Histological analysis of spinal cord neuroinflammation of WT and *Gpr109a*$^{-/-}$ mice isolated at D30 post EAE induction with Hematoxylin and eosin (H&E) staining. Scale bar for lower resolution = 100μm, and scale bar for higher resolution = 20μm.

D. Histological analysis of spinal cord demyelination of WT and *Gpr109a*$^{-/-}$ mice isolated at D30 post EAE induction with Luxol fast blue (LFB) staining. Scale bar for lower resolution = 100μm, and scale bar for higher resolution = 20μm.

(**E-F**) Proportions of inflammatory myeloid cells (CD11b^{+} CD45^{hi}) of the total leukocytes in CNS were analyzed by flow cytometry for WT and *Gpr109a*$^{-/-}$ mice. **E.** Representative flow cytometric plots of inflammatory myeloid cells in CNS from WT (left) and *Gpr109a*$^{-/-}$ (right) mice. **F.** Scatter bar chart for the proportions of inflammatory myeloid cells in CNS from WT and *Gpr109a*$^{-/-}$ mice.

(**G-H**). Proportions of Treg of the total CD4^{+} T cells in CNS of WT and *Gpr109a*$^{-/-}$ mice. **G.** Representative flow cytometric plots of Treg in CNS of WT (left) and *Gpr109a*$^{-/-}$ (right) mice. **H.** Scatter dot plots of the proportions of Treg in CNS from WT and *Gpr109a*$^{-/-}$ mice.

(**I-J**). Proportions of Treg of the total CD4^{+} T cells in spleens of WT and *Gpr109a*$^{-/-}$ mice. **I.** Representative flow cytometric plots of Treg in spleens of WT (left) and *Gpr109a*$^{-/-}$ (right) mice. **J.** Scatter dot plots of the proportions of Treg in spleens from WT and *Gpr109a*$^{-/-}$ mice.

N=11 per group for the overall study, but N=8 per group for the clinical course investigation and flow cytometry experiments. Data are presented as mean ± s.e.m. with * p<0.05, *** p<0.001, **** p<0.0001 by unpaired t-test and two-way ANOVA for the clinical curve analysis.

Figure legend for supplementary figures

Fig S1. Gating strategy to analyze Treg and Helios$^+$ Treg.

Fig S2. Gating strategy to analyze Treg and RORγt$^+$ Treg.

Fig S3. Gating strategy to analyze thymic thymopoiesis.

Fig S4. Gating strategy to analyze circulating neutrophils and their GPR109A expression.

Fig S5. Gating strategy to analyze different T cell subsets (naïve, effector, and central memory subsets).

Fig S6. Gating strategy to analyze mTECs and their expression of AIRE and GPR109A.

Fig S7. Numbers of CD4$^+$ T cells (**A**), CD8$^+$ T cells (**B**) and Treg (**C**) in the spleens of wild-type (WT) and *Gpr109a*$^{-/-}$ mice. Numbers of Treg in the mLNs (**D**) and colons (**E**) of wild-type (WT) and *Gpr109a*$^{-/-}$ mice. **F.** Numbers of Helios$^+$ Treg in the spleens of wild-type (WT) and *Gpr109a*$^{-/-}$ mice. **G.** Proportions of RORγt$^+$ Treg in the spleen of wild-type (WT) and *Gpr109a*$^{-/-}$ mice.

N=6-8 per group and data are presented as mean ± s.e.m. with * p<0.05, *** p<0.001 by unpaired t-test.

Fig S8. A. Numbers of the double-negative (DN), double-positive (DP), CD4$^+$ and CD8$^+$ T cell populations in the thymus of wild-type (WT) and *Gpr109a*$^{-/-}$ mice. **B.** Numbers of double-negative T cell subsets (DN1-DN4) in the thymus of wild-type (WT) and *Gpr109a*$^{-/-}$ mice. **C.** Numbers of Treg in the thymus of wild-type (WT) and *Gpr109a*$^{-/-}$ mice.

N=6-8 per group and data are presented as mean ± s.e.m. with * p<0.05 by unpaired t-test.

Fig S9. Expression profiles of GPR109A in T cell subsets across multiple organs. **A.** Staining of GPR109A in different splenic T cell subsets and their corresponding isotype control. **B.** Staining of GPR109A in different mLN T cell subsets and their corresponding isotype control. **C.** Staining of GPR109A in different thymic T cell subsets and their corresponding isotype control. **D.** Expression of *Gpr109a* in different immune cell subsets based on transcriptomic data from Haemosphere.

Fig S10. A. Mean fluorescence intensity (MFI) of AIRE in GPR109A$^+$ and GPR109A$^-$ mTECs. **B.** MFI of AIRE in mTECs from the thymus of wild-type (WT) and *Gpr109a*$^{-/-}$ mice.

N=6-12 per group; data are presented as mean ± s.e.m. with * $p<0.05$ by unpaired t-test.

Fig S11. A. Comprehensive analysis of gene scores for various tissue-restricted antigens (TRAs) in *Gpr109a*$^+$ and *Gpr109a*$^-$ mTECs. **B.** The top enriched gene sets of gene set enrichment analysis (GSEA) comparing *Gpr109a*$^-$ versus *Gpr109a*$^+$ mTECs based on the Hallmark gene sets. **C.** The top enriched gene sets of GSEA comparing *Gpr109a*$^-$ versus *Gpr109a*$^+$ mTECs based on the KEGG gene sets.

Fig S12. *Gpr109a*$^{-/-}$ mice show attenuated clinical signs during experimental autoimmune encephalomyelitis (EAE) compared with WT mice. A. EAE clinical course during EAE for WT (filled dots) *versus Gpr109a*$^{-/-}$ (hollow dots) mice (n=8 per group). Scatter dot plots of the days of onset of EAE (**B**), areas under the curves (AUCs) of the clinical curves (**C**), peak scores of EAE (**D**), average scores of EAE (**E**), cumulative scores of EAE (**F**) and inflammation scores of CNS (**G**) comparing WT (filled dots) versus *Gpr109a*$^{-/-}$ (hollow dots) mice during EAE.

N=8 per group, except for inflammation score analysis N=4 per group, and data are presented as mean ± s.e.m. with * $p<0.05$, ** $p<0.01$, **** $p<0.0001$ by unpaired t-test and two-way ANOVA for the clinical curve analysis.

Fig S13. Two repeated experiments showed that *Gpr109a*$^{-/-}$ mice have attenuated clinical signs during experimental autoimmune encephalomyelitis (EAE) compared with WT mice. A. EAE clinical courses

of all mice during EAE comparing WT (filled dots) versus *Gpr109a*$^{-/-}$ (hollow dots) mice (n=5-10 per group). *** p<0.005, **** p<0.0001 from two-way ANOVA for the clinical curve analysis.

Fig S14. Numbers of inflammatory myeloid cells (CD11b^{+} CD45^{hi}) (**A**) and Treg (**B**) in CNS of WT and *Gpr109a*$^{-/-}$ mice during EAE. **C.** Numbers of Treg in the spleens of WT and *Gpr109a*$^{-/-}$ mice during EAE.

N=6-8 per group; data are presented as mean ± s.e.m. with ** p<0.01 by unpaired t-test.

Fig S15. *Gpr109a*$^{-/-}$ mice show reduced antigen-specific CD4^{+} T cell responses during EAE.

(**A-C**) 2.5×10^{5} leukocytes isolated from draining lymph nodes (dLNs) from mice on D7 EAE induction were restimulated with 0/10μg/ml MOG *ex vivo* for three days. Antigen-specific responses were measured based on the carboxyfluorescein succinimidyl ester (CFSE) negative populations of CD4^{+} T cells as output of antigen-specific proliferation and the cytokine production with flow cytometry. **A.** Scatter bar chart for the proliferation index of CD4^{+} T cells from dLNs of WT and *Gpr109a*$^{-/-}$ mice restimulated with 10μg/ml MOG antigen for three days. **B.** Scatter bar chart for the proportion of Th17 in total CD4^{+} T cells in dLNs of WT and *Gpr109a*$^{-/-}$ mice after 10μg/ml MOG *ex vivo* stimulation for three days. **C.** Scatter bar chart for IL-17 concentration in the culture supernatant of leukocytes from dLNs restimulated with 10μg/ml MOG *ex vivo* for three days determined by ELISA.

N=3 per group; data are presented as mean ± s.e.m., with * p<0.05 by unpaired t-test.

Tables

Table 1. Key reagents and resources used in this study.

Reagent	Source	Identifier
Antibodies		
Anti-mouse CD45 BV785 (Clone 30-F11)	BioLegend	Cat# 103149; RRID: AB_2564590
Anti-mouse CD4 PerCP/Cy5.5 (Clone GK1.5)	BioLegend	Cat# 100434; RRID: AB_893324
Anti-mouse CD8a BV650 (Clone 53-6.7)	BioLegend	Cat# 100742; RRID: AB_2563056
Anti-mouse CD25 BV605 (Clone PC61)	BD	Cat# 563061; RRID: AB_2737982
Anti-mouse FOXP3 APC (Clone REA788)	Miltenyi	Cat# 130-111-601; RRID: AB_2651770
Anti-mouse CD44 APC/CY7 (Clone IM7)	BioLegend	Cat# 103028; RRID: AB_830785
Anti-mouse Ly6G BV650 (Clone 1A8)	BioLegend	Cat# 127641; RRID: AB_2565881
Anti-mouse CD3 AF488 (Clone 17A2)	BioLegend	Cat# 100210; RRID: AB_389301
Anti-mouse Helios PE (Clone REA829)	Miltenyi	Cat# 130-112-630; RRID: AB_2651980

Anti-mouse CD45 PERCP (Clone 30-F11)	BioLegend	Cat# 103130; RRID: AB_893339
Anti-mouse CD3 BV711 (Clone 17A2)	BioLegend	Cat# 100241; RRID: AB_2563945
Anti-mouse CD4 BV750 (Clone GK1.5)	BioLegend	Cat#100467; RRID: AB_2734150
Anti-mouse FOXP3 Vio515 (Clone REA788)	Miltenyi	Cat# 130-111-603; RRID: AB_2651770
Anti-mouse RORγt PE	eBioscience	Cat# 12-6981-80; RRID: AB_10807092
Anti-mouse EpCAM APC (Clone G8.8)	BioLegend	Cat# 118214; RRID: AB_1134102
Anti-mouse MHC-II BV510 (Clone 2G9)	BD	Cat# 743871; RRID: AB_2741822
Anti-mouse Ly51 PERCP/Cy5.5 (Clone 6C3)	BioLegend	Cat# 108316; RRID: AB_2632658
Anti-mouse AIRE AF488 (Clone 5H12)	eBioscience	Cat# 53-5934-82, RRID: AB_10854132
Anti-mouse Ly6G AF647	BioLegend	Cat# 127610; RRID: AB_1134159

Anti-mouse CD3 PE/CF594 (Clone 145-2C11)	BD	Cat# 562286; RRID: AB_11153307
Anti-mouse γδTCR BV421 (Clone GL3)	BioLegend	Cat# 118120; RRID: AB_2562566
Anti-mouse γδTCR PE/CY5 (Clone GL3)	eBioscience	Cat# 15-5711-82; RRID: AB_468804
Anti-mouse CD62L BV421 (Clone MEL-14)	BioLegend	Cat# 104436; RRID: AB_2562560
Anti-mouse IL-17 PE (Clone REA660)	Miltenyi	Cat#130-112-009; RRID: AB_2652360
Anti-mouse IFNγ BV650 (Clone XMG1.2)	BioLegend	Cat# 505832; RRID: AB_2734492
Anti-mouse CD11b BUV395 (Clone M1/70)	BD	Cat# 563553; RRID: AB_1134159
Strepavidin PE (biotinylated)	Miltenyi	Cat# 130-106-789; RRID: AB_2734492
Mouse IgG2c-UNLB (6.3)	Southern Biotech	Cat# 0122-01; RRID: AB_2794064
Anti-mouse IL-17A	BioLegend	Cat# 506901; RRID: AB_315461
Biotin anti-mouse IL-17A	BioLegend	Cat# 507002; RRID: AB_315466
Chemicals, and peptides		

Myelin oligodendrocyte glycoprotein 35-55 (MOG, MEV GWY RSP FSR VVH LYR NGK)	GenScript	Cat# 163913-87-9
Pertussis toxin from *Bordetella pertussis*	Sigma	Cat# P7208
Incomplete Freund's adjuvant (IFA)	Chondrex, Inc.	Cat# 7002
PBS	Thermo Fisher Scientific	Cat# 18912014
Hank's balanced salt solution (HBSS)	Thermo Fisher Scientific	Cat# 24020117
RPMI-1640	Thermo Fisher Scientific	Cat# 21870092
Phorbol 12-myristate 13-acetate	Sigma-Aldrich	Cat# P8139
Ionomycin calcium salt from Streptomyces conglobatus	Sigma-Aldrich	Cat# I0634
Brefeldin A	BioLegend	Cat# 420601
Penicillin/Streptomycin	Sigma-Aldrich	Cat# 15140122
HEPES buffer	Thermo Fisher Scientific	Cat# 15630080
Collagenase type IV	Thermo Fisher Scientific	Cat# 17104019
Percoll ®	Cytiva	Cat# 17089101
Foetal Bovine Serum	Bovogen Biologicals	Cat# AFBS-500

Critical commercial assays		
LIVE/DEAD™ Fixable Blue Dead Cell Stain Kit, for UV excitation	Thermo Fisher Scientific	Cat# L34962
Deposited data		
Single cell RNA sequencing data from mouse medullary thymic epithelial cells	(44)	Accession: GSE131339
Single cell RNA sequencing data from human thymic stroma	(45)	Accession: GSE147520
Experimental models: Organisms/strains		
Mus muculus (C57BL/6)	Australian BioResources	JAX:000664
***Gpr109a*$^{-/-}$ mice**		
Mycobacterium tuberculosis Des. H37 Rα	BD	Cat# 231141
Sp2/0-Ag14 cell line	ATCC	CRL-1581
Software and algorithms		
Graphpad Prism v10	GraphPad Software	RRID:SCR_008520
R Project for Statistical Computing	R Foundation	RRID:SCR_001905
RStudio	RStudio	RRID:SCR_000432
FlowJo v10	FlowJo Inc.	RRID:SCR_008520
Seurat 4.1.0.	(46-48)	RRID:SCR_016341

626

627 **Table 2. Scoring guideline for the EAE clinical signs.**

Clinical EAE Score	Signs
0	No signs of disease
1	Loss of tail tonus
2	Hind limb weakness
3	Hind limb paralysis
4	Paralysis of one forelimb
5	Paralysis of both forelimbs, moribund or dead

628

629 **Table 3. Scoring system for the CNS inflammation of spinal cord sections from EAE mice.**

Score	Inflammation
0	No inflammation or infiltration
1	A few inflammatory cells present in the leptomeninges
2	Organisation of infiltrates around the blood vessels
3	Extensive perivascular cuffing and extension into the underlying parenchyma
4	Infiltration in the parenchymal region, less than half of total white matter
5	Extensive infiltration in the parenchymal region, more than half of total white matter

630

631

632

633

References

1. Dejaco C, Duftner C, Grubeck-Loebenstein B, Schirmer M. Imbalance of regulatory T cells in human autoimmune diseases. Immunology. 2006;117(3):289-300. http://10.1111/j.1365-2567.2005.02317.x.
2. Dominguez-Villar M, Hafler DA. Regulatory T cells in autoimmune disease. Nat Immunol. 2018;19(7):665-73. http://10.1038/s41590-018-0120-4.
3. Kitz A, Singer E, Hafler D. Regulatory T Cells: From Discovery to Autoimmunity. Cold Spring Harb Perspect Med. 2018;8(12). http://10.1101/cshperspect.a029041.
4. Rana J, Biswas M. Regulatory T cell therapy: Current and future design perspectives. Cell Immunol. 2020;356:104193. http://10.1016/j.cellimm.2020.104193.
5. Brunstein CG, Miller JS, Cao Q, McKenna DH, Hippen KL, Curtsinger J, et al. Infusion of ex vivo expanded T regulatory cells in adults transplanted with umbilical cord blood: safety profile and detection kinetics. Blood. 2011;117(3):1061-70. http://10.1182/blood-2010-07-293795.
6. Trzonkowski P, Bieniaszewska M, Juscinska J, Dobyszuk A, Krzystyniak A, Marek N, et al. First-in-man clinical results of the treatment of patients with graft versus host disease with human ex vivo expanded CD4+CD25+CD127- T regulatory cells. Clin Immunol. 2009;133(1):22-6. http://10.1016/j.clim.2009.06.001.
7. Voskens C, Stoica D, Rosenberg M, Vitali F, Zundler S, Ganslmayer M, et al. Autologous regulatory T-cell transfer in refractory ulcerative colitis with concomitant primary sclerosing cholangitis. Gut. 2022. http://10.1136/gutjnl-2022-327075.
8. Duffy SS, Keating BA, Moalem-Taylor G. Adoptive Transfer of Regulatory T Cells as a Promising Immunotherapy for the Treatment of Multiple Sclerosis. Front Neurosci. 2019;13:1107. http://10.3389/fnins.2019.01107.
9. Sakaguchi S, Wing K, Yamaguchi T. Dynamics of peripheral tolerance and immune regulation mediated by Treg. Eur J Immunol. 2009;39(9):2331-6. http://10.1002/eji.200939688.
10. Savage PA, Klawon DEJ, Miller CH. Regulatory T Cell Development. Annu Rev Immunol. 2020;38:421-53. http://10.1146/annurev-immunol-100219-020937.
11. Kanamori M, Nakatsukasa H, Okada M, Lu Q, Yoshimura A. Induced Regulatory T Cells: Their Development, Stability, and Applications. Trends Immunol. 2016;37(11):803-11. http://10.1016/j.it.2016.08.012.
12. Thornton AM, Korty PE, Tran DQ, Wohlfert EA, Murray PE, Belkaid Y, et al. Expression of Helios, an Ikaros transcription factor family member, differentiates thymic-derived from peripherally induced Foxp3+ T regulatory cells. J Immunol. 2010;184(7):3433-41. http://10.4049/jimmunol.0904028.
13. Owen DL, Sjaastad LE, Farrar MA. Regulatory T Cell Development in the Thymus. J Immunol. 2019;203(8):2031-41. http://10.4049/jimmunol.1900662.
14. Santamaria JC, Borelli A, Irla M. Regulatory T Cell Heterogeneity in the Thymus: Impact on Their Functional Activities. Front Immunol. 2021;12:643153. http://10.3389/fimmu.2021.643153.
15. Anderson MS, Venanzi ES, Klein L, Chen Z, Berzins SP, Turley SJ, et al. Projection of an immunological self shadow within the thymus by the aire protein. Science. 2002;298(5597):1395-401. http://10.1126/science.1075958.
16. Jiang W, Anderson MS, Bronson R, Mathis D, Benoist C. Modifier loci condition autoimmunity provoked by Aire deficiency. J Exp Med. 2005;202(6):805-15. http://10.1084/jem.20050693.
17. Derbinski J, Gabler J, Brors B, Tierling S, Jonnakuty S, Hergenhahn M, et al. Promiscuous gene expression in thymic epithelial cells is regulated at multiple levels. J Exp Med. 2005;202(1):33-45. http://10.1084/jem.20050471.
18. Sansom SN, Shikama-Dorn N, Zhanybekova S, Nusspaumer G, Macaulay IC, Deadman ME, et al. Population and single-cell genomics reveal the Aire dependency, relief from Polycomb silencing, and

680 distribution of self-antigen expression in thymic epithelia. Genome Res. 2014;24(12):1918-31.
681 http://10.1101/gr.171645.113.
682 19. Cowan JE, Baik S, McCarthy NI, Parnell SM, White AJ, Jenkinson WE, et al. Aire controls the
683 recirculation of murine Foxp3(+) regulatory T-cells back to the thymus. Eur J Immunol. 2018;48(5):844-54.
684 http://10.1002/eji.201747375.
685 20. Yang S, Fujikado N, Kolodin D, Benoist C, Mathis D. Immune tolerance. Regulatory T cells
686 generated early in life play a distinct role in maintaining self-tolerance. Science. 2015;348(6234):589-94.
687 http://10.1126/science.aaa7017.
688 21. Kekalainen E, Tuovinen H, Joensuu J, Gylling M, Franssila R, Pontynen N, et al. A defect of
689 regulatory T cells in patients with autoimmune polyendocrinopathy-candidiasis-ectodermal dystrophy. J
690 Immunol. 2007;178(2):1208-15. http://10.4049/jimmunol.178.2.1208.
691 22. Aschenbrenner K, D'Cruz LM, Vollmann EH, Hinterberger M, Emmerich J, Swee LK, et al. Selection
692 of Foxp3+ regulatory T cells specific for self antigen expressed and presented by Aire+ medullary thymic
693 epithelial cells. Nat Immunol. 2007;8(4):351-8. http://10.1038/ni1444.
694 23. Takaba H, Morishita Y, Tomofuji Y, Danks L, Nitta T, Komatsu N, et al. Fezf2 Orchestrates a Thymic
695 Program of Self-Antigen Expression for Immune Tolerance. Cell. 2015;163(4):975-87.
696 http://10.1016/j.cell.2015.10.013.
697 24. Yadav M, Stephan S, Bluestone JA. Peripherally induced tregs - role in immune homeostasis and
698 autoimmunity. Front Immunol. 2013;4:232. http://10.3389/fimmu.2013.00232.
699 25. Atarashi K, Tanoue T, Shima T, Imaoka A, Kuwahara T, Momose Y, et al. Induction of colonic
700 regulatory T cells by indigenous Clostridium species. Science. 2011;331(6015):337-41.
701 http://10.1126/science.1198469.
702 26. Tan J, McKenzie C, Potamitis M, Thorburn AN, Mackay CR, Macia L. The role of short-chain fatty
703 acids in health and disease. Adv Immunol. 2014;121:91-119. http://10.1016/B978-0-12-800100-4.00003-
704 9.
705 27. Tan J, Taitz J, Sun SM, Langford L, Ni D, Macia L. Your Regulatory T Cells Are What You Eat: How
706 Diet and Gut Microbiota Affect Regulatory T Cell Development. Front Nutr. 2022;9:878382.
707 http://10.3389/fnut.2022.878382.
708 28. Tan JK, McKenzie C, Marino E, Macia L, Mackay CR. Metabolite-Sensing G Protein-Coupled
709 Receptors-Facilitators of Diet-Related Immune Regulation. Annu Rev Immunol. 2017;35:371-402.
710 http://10.1146/annurev-immunol-051116-052235.
711 29. Smith PM, Howitt MR, Panikov N, Michaud M, Gallini CA, Bohlooly YM, et al. The microbial
712 metabolites, short-chain fatty acids, regulate colonic Treg cell homeostasis. Science. 2013;341(6145):569-
713 73. http://10.1126/science.1241165.
714 30. Daien CI, Tan J, Audo R, Mielle J, Quek LE, Krycer JR, et al. Gut-derived acetate promotes B10 cells
715 with antiinflammatory effects. JCI Insight. 2021;6(7). http://10.1172/jci.insight.144156.
716 31. Tan J, McKenzie C, Vuillermin PJ, Goverse G, Vinuesa CG, Mebius RE, et al. Dietary Fiber and
717 Bacterial SCFA Enhance Oral Tolerance and Protect against Food Allergy through Diverse Cellular Pathways.
718 Cell Rep. 2016;15(12):2809-24. http://10.1016/j.celrep.2016.05.047.
719 32. Singh N, Gurav A, Sivaprakasam S, Brady E, Padia R, Shi H, et al. Activation of Gpr109a, receptor
720 for niacin and the commensal metabolite butyrate, suppresses colonic inflammation and carcinogenesis.
721 Immunity. 2014;40(1):128-39. http://10.1016/j.immuni.2013.12.007.
722 33. Macia L, Tan J, Vieira AT, Leach K, Stanley D, Luong S, et al. Metabolite-sensing receptors GPR43
723 and GPR109A facilitate dietary fibre-induced gut homeostasis through regulation of the inflammasome.
724 Nat Commun. 2015;6:6734. http://10.1038/ncomms7734.
725 34. Pinget GV, Tan JK, Ni D, Taitz J, Daien CI, Mielle J, et al. Dysbiosis in imiquimod-induced psoriasis
726 alters gut immunity and exacerbates colitis development. Cell Rep. 2022;40(7):111191.
727 http://10.1016/j.celrep.2022.111191.

35. Seach N, Hammett M, Chidgey A. Isolation, characterization, and reaggregate culture of thymic epithelial cells. Methods Mol Biol. 2013;945:251-72. http://10.1007/978-1-62703-125-7_15.

36. Yano M, Kuroda N, Han H, Meguro-Horike M, Nishikawa Y, Kiyonari H, et al. Aire controls the differentiation program of thymic epithelial cells in the medulla for the establishment of self-tolerance. J Exp Med. 2008;205(12):2827-38. http://10.1084/jem.20080046.

37. Felizardo RJF, de Almeida DC, Pereira RL, Watanabe IKM, Doimo NTS, Ribeiro WR, et al. Gut microbial metabolite butyrate protects against proteinuric kidney disease through epigenetic- and GPR109a-mediated mechanisms. FASEB J. 2019;33(11):11894-908. http://10.1096/fj.201901080R.

38. Piccio L, Stark JL, Cross AH. Chronic calorie restriction attenuates experimental autoimmune encephalomyelitis. J Leukoc Biol. 2008;84(4):940-8. http://10.1189/jlb.0208133.

39. Cignarella F, Cantoni C, Ghezzi L, Salter A, Dorsett Y, Chen L, et al. Intermittent Fasting Confers Protection in CNS Autoimmunity by Altering the Gut Microbiota. Cell Metab. 2018;27(6):1222-35 e6. http://10.1016/j.cmet.2018.05.006.

40. Choi IY, Piccio L, Childress P, Bollman B, Ghosh A, Brandhorst S, et al. A Diet Mimicking Fasting Promotes Regeneration and Reduces Autoimmunity and Multiple Sclerosis Symptoms. Cell Rep. 2016;15(10):2136-46. http://10.1016/j.celrep.2016.05.009.

41. Choi J, Baldwin TM, Wong M, Bolden JE, Fairfax KA, Lucas EC, et al. Haemopedia RNA-seq: a database of gene expression during haematopoiesis in mice and humans. Nucleic Acids Res. 2019;47(D1):D780-D5. http://10.1093/nar/gky1020.

42. de Graaf CA, Choi J, Baldwin TM, Bolden JE, Fairfax KA, Robinson AJ, et al. Haemopedia: An Expression Atlas of Murine Hematopoietic Cells. Stem Cell Reports. 2016;7(3):571-82. http://10.1016/j.stemcr.2016.07.007.

43. Stephenson L, Wakeham Y, Seidenman N, Choi J. Building online genomics applications using BioPyramid. Bioinformatics. 2018;34(17):3055-7. http://10.1093/bioinformatics/bty207.

44. Cowan JE, Malin J, Zhao Y, Seedhom MO, Harly C, Ohigashi I, et al. Myc controls a distinct transcriptional program in fetal thymic epithelial cells that determines thymus growth. Nat Commun. 2019;10(1):5498. http://10.1038/s41467-019-13465-y.

45. Bautista JL, Cramer NT, Miller CN, Chavez J, Berrios DI, Byrnes LE, et al. Single-cell transcriptional profiling of human thymic stroma uncovers novel cellular heterogeneity in the thymic medulla. Nat Commun. 2021;12(1):1096. http://10.1038/s41467-021-21346-6.

46. Hao Y, Hao S, Andersen-Nissen E, Mauck WM, 3rd, Zheng S, Butler A, et al. Integrated analysis of multimodal single-cell data. Cell. 2021;184(13):3573-87 e29. http://10.1016/j.cell.2021.04.048.

47. Stuart T, Butler A, Hoffman P, Hafemeister C, Papalexi E, Mauck WM, 3rd, et al. Comprehensive Integration of Single-Cell Data. Cell. 2019;177(7):1888-902 e21. http://10.1016/j.cell.2019.05.031.

48. Butler A, Hoffman P, Smibert P, Papalexi E, Satija R. Integrating single-cell transcriptomic data across different conditions, technologies, and species. Nat Biotechnol. 2018;36(5):411-20. http://10.1038/nbt.4096.

49. Love MI, Huber W, Anders S. Moderated estimation of fold change and dispersion for RNA-seq data with DESeq2. Genome Biol. 2014;15(12):550. http://10.1186/s13059-014-0550-8.

50. Subramanian A, Tamayo P, Mootha VK, Mukherjee S, Ebert BL, Gillette MA, et al. Gene set enrichment analysis: a knowledge-based approach for interpreting genome-wide expression profiles. Proc Natl Acad Sci U S A. 2005;102(43):15545-50. http://10.1073/pnas.0506580102.

51. Korotkevich G, Sukhov V, Budin N, Shpak B, Artyomov MN, Sergushichev A. Fast gene set enrichment analysis. 2021. http://10.1101/060012.

52. Baran-Gale J, Morgan MD, Maio S, Dhalla F, Calvo-Asensio I, Deadman ME, et al. Ageing compromises mouse thymus function and remodels epithelial cell differentiation. Elife. 2020;9. http://10.7554/eLife.56221.

53. Zegarra-Ruiz DF, Kim DV, Norwood K, Kim M, Wu WH, Saldana-Morales FB, et al. Thymic development of gut-microbiota-specific T cells. Nature. 2021;594(7863):413-7. http://10.1038/s41586-021-03531-1.
54. Yang BH, Hagemann S, Mamareli P, Lauer U, Hoffmann U, Beckstette M, et al. Foxp3(+) T cells expressing RORgammat represent a stable regulatory T-cell effector lineage with enhanced suppressive capacity during intestinal inflammation. Mucosal Immunol. 2016;9(2):444-57. http://10.1038/mi.2015.74.
55. Klein L, Kyewski B, Allen PM, Hogquist KA. Positive and negative selection of the T cell repertoire: what thymocytes see (and don't see). Nat Rev Immunol. 2014;14(6):377-91. http://10.1038/nri3667.
56. Wang HX, Pan W, Zheng L, Zhong XP, Tan L, Liang Z, et al. Thymic Epithelial Cells Contribute to Thymopoiesis and T Cell Development. Front Immunol. 2019;10:3099. http://10.3389/fimmu.2019.03099.
57. Sakaguchi S, Miyara M, Costantino CM, Hafler DA. FOXP3+ regulatory T cells in the human immune system. Nat Rev Immunol. 2010;10(7):490-500. http://10.1038/nri2785.
58. Josefowicz SZ, Lu LF, Rudensky AY. Regulatory T cells: mechanisms of differentiation and function. Annu Rev Immunol. 2012;30:531-64. http://10.1146/annurev.immunol.25.022106.141623.
59. Viglietta V, Baecher-Allan C, Weiner HL, Hafler DA. Loss of functional suppression by CD4+CD25+ regulatory T cells in patients with multiple sclerosis. J Exp Med. 2004;199(7):971-9. http://10.1084/jem.20031579.
60. Kimura K. Regulatory T cells in multiple sclerosis. Clinical and Experimental Neuroimmunology. 2020;11(3):148-55. http://10.1111/cen3.12591.
61. Chen X, Fang L, Song S, Guo TB, Liu A, Zhang JZ. Thymic regulation of autoimmune disease by accelerated differentiation of Foxp3+ regulatory T cells through IL-7 signaling pathway. J Immunol. 2009;183(10):6135-44. http://10.4049/jimmunol.0901576.
62. Akirav EM, Bergman CM, Hill M, Ruddle NH. Depletion of CD4(+)CD25(+) T cells exacerbates experimental autoimmune encephalomyelitis induced by mouse, but not rat, antigens. J Neurosci Res. 2009;87(15):3511-9. http://10.1002/jnr.21981.
63. Docampo MD, da Silva MB, Lazrak A, Nichols KB, Lieberman SR, Slingerland AE, et al. Alloreactive T cells deficient of the short-chain fatty acid receptor GPR109A induce less graft-versus-host disease. Blood. 2022;139(15):2392-405. http://10.1182/blood.2021010719.
64. Hu M, Eviston D, Hsu P, Marino E, Chidgey A, Santner-Nanan B, et al. Decreased maternal serum acetate and impaired fetal thymic and regulatory T cell development in preeclampsia. Nat Commun. 2019;10(1):3031. http://10.1038/s41467-019-10703-1.
65. Nakajima A, Kaga N, Nakanishi Y, Ohno H, Miyamoto J, Kimura I, et al. Maternal High Fiber Diet during Pregnancy and Lactation Influences Regulatory T Cell Differentiation in Offspring in Mice. J Immunol. 2017;199(10):3516-24. http://10.4049/jimmunol.1700248.
66. Tunaru S, Kero J, Schaub A, Wufka C, Blaukat A, Pfeffer K, et al. PUMA-G and HM74 are receptors for nicotinic acid and mediate its anti-lipolytic effect. Nat Med. 2003;9(3):352-5. http://10.1038/nm824.
67. Taggart AK, Kero J, Gan X, Cai TQ, Cheng K, Ippolito M, et al. (D)-beta-Hydroxybutyrate inhibits adipocyte lipolysis via the nicotinic acid receptor PUMA-G. J Biol Chem. 2005;280(29):26649-52. http://10.1074/jbc.C500213200.
68. Thorburn AN, McKenzie CI, Shen S, Stanley D, Macia L, Mason LJ, et al. Evidence that asthma is a developmental origin disease influenced by maternal diet and bacterial metabolites. Nat Commun. 2015;6:7320. http://10.1038/ncomms8320.
69. Sugimoto M, Ikeda S, Niigata K, Tomita M, Sato H, Soga T. MMMDB: Mouse Multiple Tissue Metabolome Database. Nucleic Acids Res. 2012;40(Database issue):D809-14. http://10.1093/nar/gkr1170.
70. Hirschberger S, Strauss G, Effinger D, Marstaller X, Ferstl A, Muller MB, et al. Very-low-carbohydrate diet enhances human T-cell immunity through immunometabolic reprogramming. EMBO Mol Med. 2021;13(8):e14323. http://10.15252/emmm.202114323.

71. Hu S, Liu L, Chang EB, Wang JY, Raufman JP. Butyrate inhibits pro-proliferative miR-92a by diminishing c-Myc-induced miR-17-92a cluster transcription in human colon cancer cells. Mol Cancer. 2015;14:180. http://10.1186/s12943-015-0450-x.
72. Subramani K, Chu X, Warren M, Lee M, Lu S, Singh N, et al. Deficiency of metabolite sensing receptor HCA2 impairs the salutary effect of niacin in hemorrhagic shock. Biochim Biophys Acta Mol Basis Dis. 2019;1865(3):688-95. http://10.1016/j.bbadis.2019.01.009.
73. Liu H, Feng XD, Yang B, Tong RL, Lu YJ, Chen DY, et al. Dimethyl fumarate suppresses hepatocellular carcinoma progression via activating SOCS3/JAK1/STAT3 signaling pathway. Am J Transl Res. 2019;11(8):4713-25.
74. Goldfarb Y, Kadouri N, Levi B, Sela A, Herzig Y, Cohen RN, et al. HDAC3 Is a Master Regulator of mTEC Development. Cell Rep. 2016;15(3):651-65. http://10.1016/j.celrep.2016.03.048.
75. Heinlein M, Gandolfo LC, Zhao K, Teh CE, Nguyen N, Baell JB, et al. The acetyltransferase KAT7 is required for thymic epithelial cell expansion, expression of AIRE target genes, and thymic tolerance. Sci Immunol. 2022;7(67):eabb6032. http://10.1126/sciimmunol.abb6032.
76. Duscha A, Gisevius B, Hirschberg S, Yissachar N, Stangl GI, Eilers E, et al. Propionic Acid Shapes the Multiple Sclerosis Disease Course by an Immunomodulatory Mechanism. Cell. 2020;180(6):1067-80 e16. http://10.1016/j.cell.2020.02.035.
77. Dobbins RL, Shearn SP, Byerly RL, Gao FF, Mahar KM, Napolitano A, et al. GSK256073, a selective agonist of G-protein coupled receptor 109A (GPR109A) reduces serum glucose in subjects with type 2 diabetes mellitus. Diabetes Obes Metab. 2013;15(11):1013-21. http://10.1111/dom.12132.
78. Offermanns S. The nicotinic acid receptor GPR109A (HM74A or PUMA-G) as a new therapeutic target. Trends Pharmacol Sci. 2006;27(7):384-90. http://10.1016/j.tips.2006.05.008.

Figures

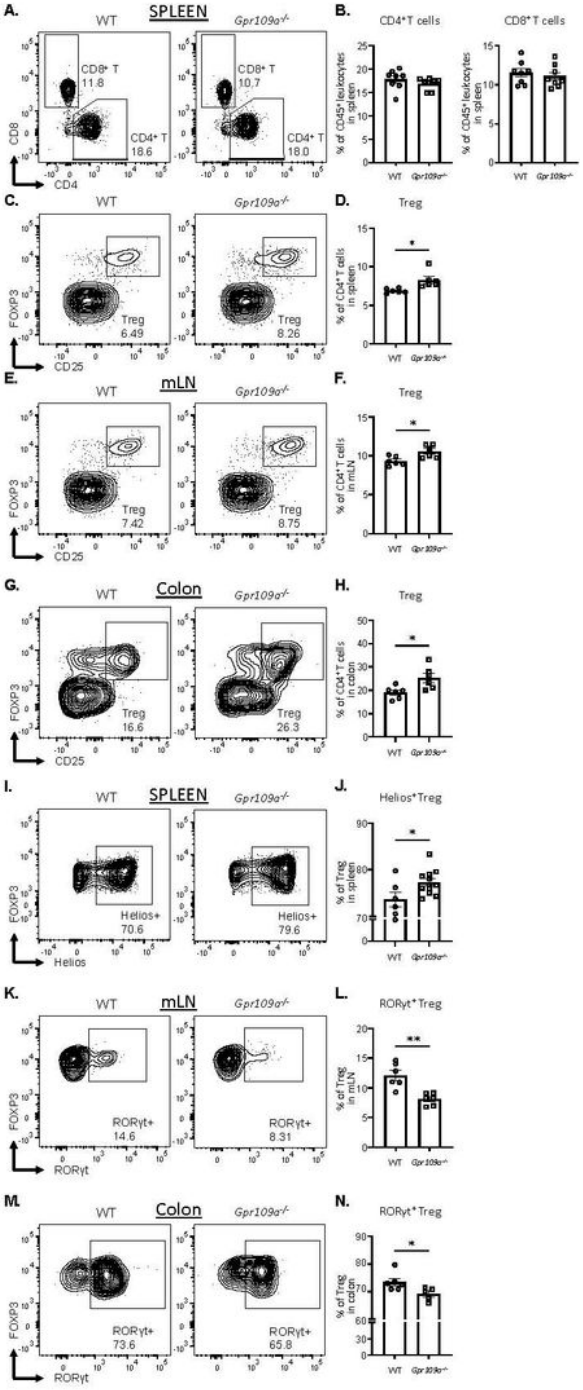

Figure 1

Gpr109a−/−mice showed Treg imbalance with increased thymic derived Treg and decreased microbiota-induced Treg.

(A-B) Proportions of CD4+ and CD8+ T cells in total leukocytes (CD45+) were analyzed by flow cytometry in spleens of wild-type (WT) and Gpr109a-/- mice. A. Representative flow cytometric plots of spleen CD4+ and CD8+ T cells in WT (left) and Gpr109a-/- (right) mice. B. Scatter bar chart for the proportions of CD4+ and CD8+ T cells in spleens from WT and Gpr109a-/- mice.

(C-H) Proportions of regulatory T cells (Treg) in total CD4+ T cells of WT (left) and Gpr109a-/- (right) mice and their representative flow cytometric plots in spleen (C-D), mesenteric lymph nodes (mLNs) (E-F) and colon (G-H) respectively.

(I-J) Proportions of thymic derived (Helios+) Treg among total Treg population in spleens of WT (left) and Gpr109a-/- (right) mice. I. Representative flow cytometric plots of Helios+ Treg in WT (left) and Gpr109a-/- (right) mice. J. Scatter bar chart for the proportions of Helios+ Treg in spleens from WT and Gpr109a-/- mice.

(K-L) Proportions of microbiota-induced (ROR?t+) Treg among total Treg population in mLNs of WT (left) and Gpr109a-/- (right) mice. K. Representative flow cytometric plots of RORγt+ Treg in WT (left) and Gpr109a-/- (right) mice. L. Scatter bar chart for the proportions of RORγt+ Treg in mLNs from WT and Gpr109a-/- mice.

(M-N) Proportions of microbiota-induced (ROR?t+) Treg among total Treg population in colon of WT (left) and Gpr109a-/- (right) mice. M. Representative flow cytometric plots of RORγt+ Treg in WT (left) and Gpr109a-/- (right) mice. N. Scatter bar chart for the proportions of RORγt+ Treg in colon from WT and Gpr109a-/- mice. N=6-8 per group and data are presented as mean ± s.e.m. with * $p<0.05$, ** $p<0.01$, *** $p<0.001$ by unpaired t-test.

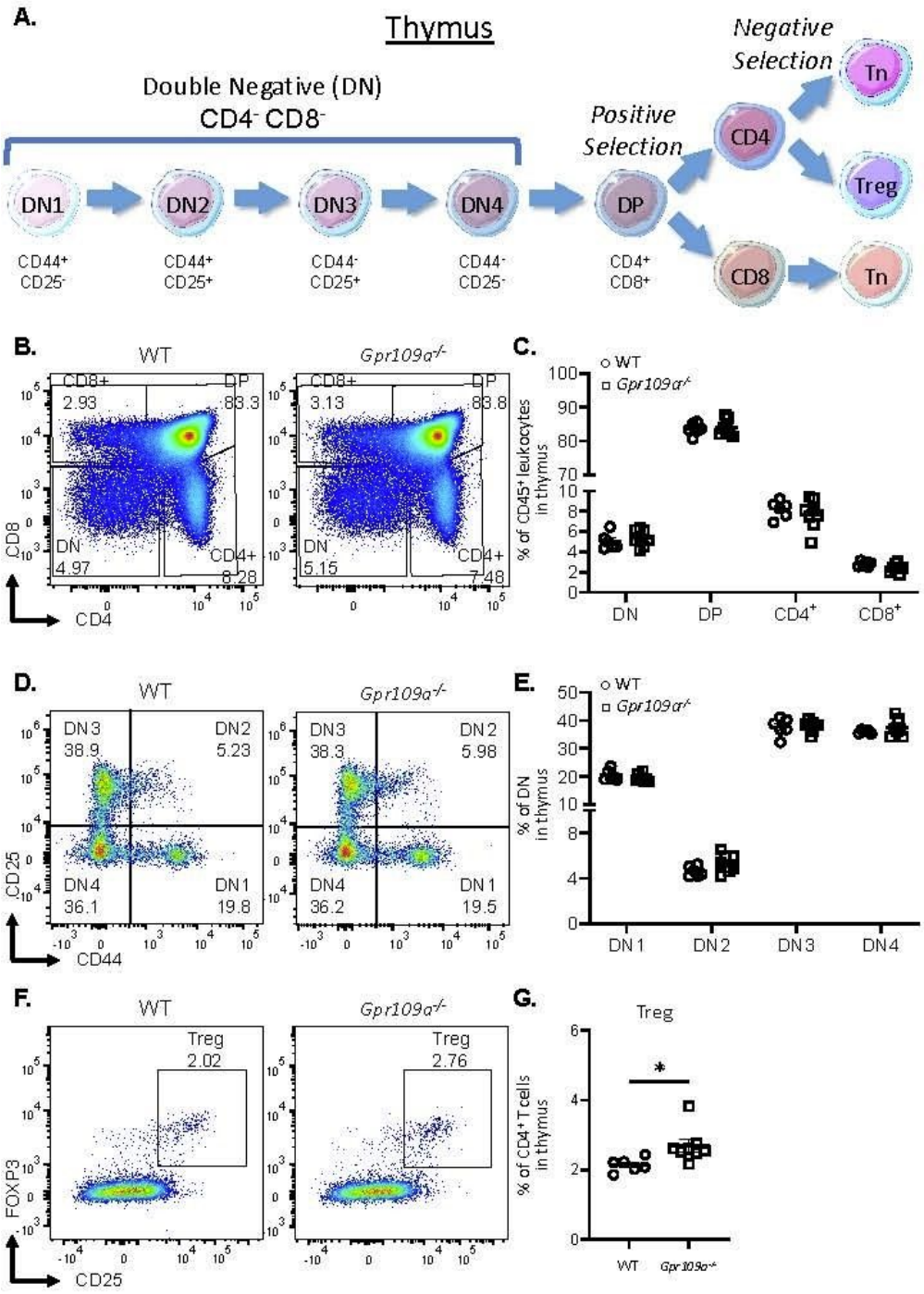

Figure 2

Gpr109a−/−mice showed increased thymic Treg generation but not thymopoiesis.

A. An overview of the thymopoiesis process.

(B-C) Proportions of double-negative (DN), double-positive (DP), CD4+ and CD8+ T cells in total leukocytes (CD45+) were analyzed by flow cytometry in thymus of wild-type (WT) and Gpr109a−/− mice. B. Representative flow cytometric plots of thymus DN, DP, CD4+ and CD8+ T cells in WT (left) and Gpr109a−/− (right) mice. C. Scatter dot plots of the proportions of DN, DP, CD4+ and CD8+ T cells in thymus from WT and Gpr109a−/− mice.

(D-E) Proportions of double-negative one to four (DN1-DN4) populations in total DN T cells in thymus of wild-type (WT) and Gpr109a−/− mice. D. Representative flow cytometric plots of thymus DN1-DN4 populations in WT (left) and Gpr109a−/− (right) mice. E. Scatter dot plots of the proportions of DN1-DN4 populations in thymus from WT and Gpr109a−/− mice.

(F-G) Proportions of Treg in total CD4+ T cells in thymus of wild-type (WT) and Gpr109a−/− mice. F. Representative flow cytometric plots of thymus Treg in WT (left) and Gpr109a−/− (right) mice. G. Scatter dot plots of the proportions of Treg in thymus from WT and Gpr109a−/− mice.

N=6-8 per group and data are presented as mean ± s.e.m. with ** $p<0.01$ by unpaired t-test.

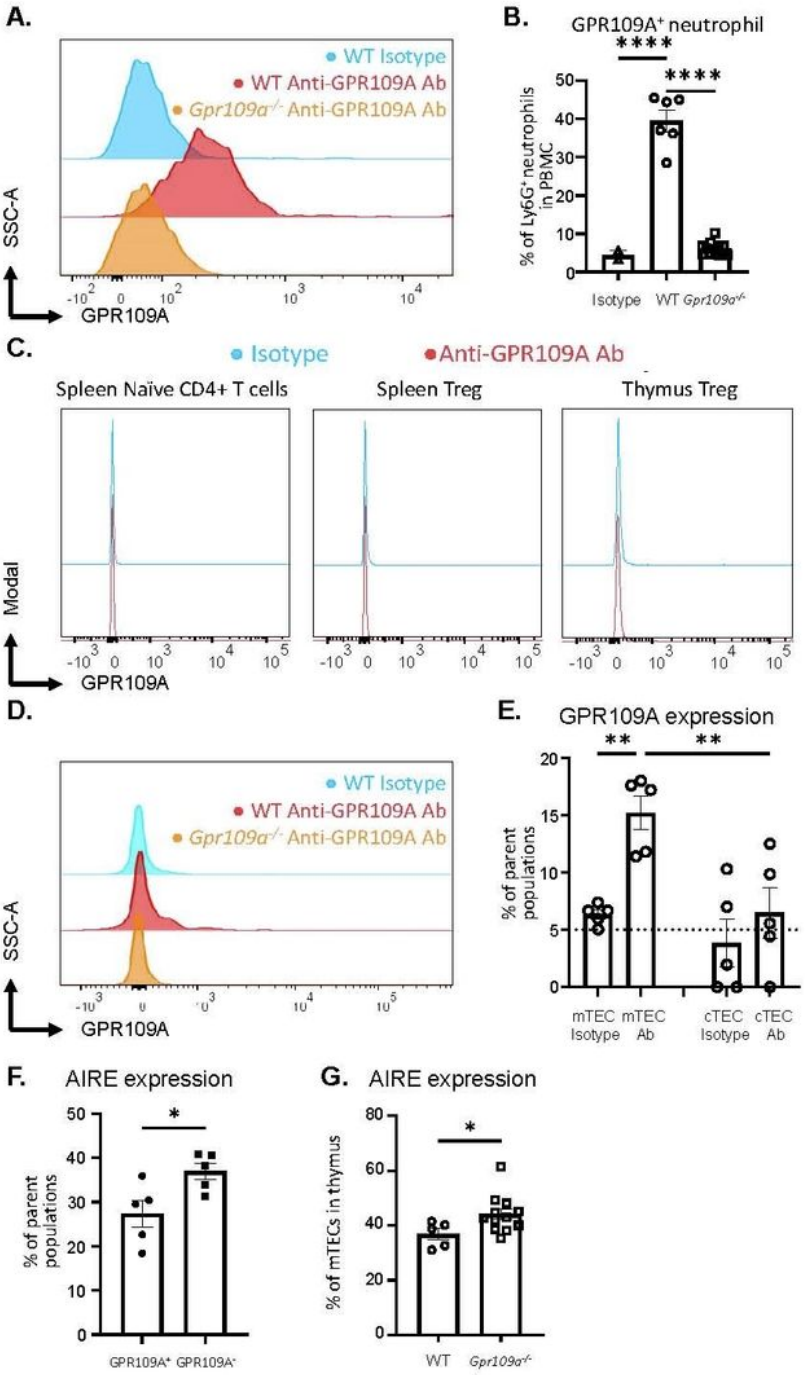

Figure 3

GPR109A was not expressed in T cells but in thymic medullary epithelial cells (mTECs) and was associated with reduced AIRE expression.

(A-B) Staining of GPR109A in circulating mouse neutrophils. A. Histogram for staining of GPR109A in circulating mouse neutrophils (Ly6G+) in WT (red) and Gpr109a−/− (orange) mice and the isotype control

for the monoclonal Ab (cyan). B. Scatter bar chart for the proportions of GPR109A+ neutrophils in WT and Gpr109a−/− mice and the isotype control for the monoclonal Ab.

(C) Histograms for staining of GPR109A in splenic naïve CD4+ T cells, splenic Treg and thymic Treg and their corresponding isotype control.

(D-E) Staining of GPR109A in thymic medullary epithelial cells (mTECs). D. Histogram for staining of GPR109A in mTECs in WT (red) and Gpr109a−/− (orange) mice and the isotype control for the monoclonal Ab (cyan). E. Scatter bar chart for the proportions of GPR109A+ mTECs and cTECs in WT mice and the corresponding isotype control for the monoclonal Ab.

F. Scatter bar chart of the proportions of AIRE+ mTECs from GPR109A+ mTECs versus GPR109A- mTECs.

G. Scatter bar chart of the proportions of AIRE+ mTECs in WT and Gpr109a−/− mice.

N=5-8 per group and data are presented as mean ± s.e.m. with * $p<0.05$, *** $p<0.001$, **** $p<0.0001$ by unpaired t-test.

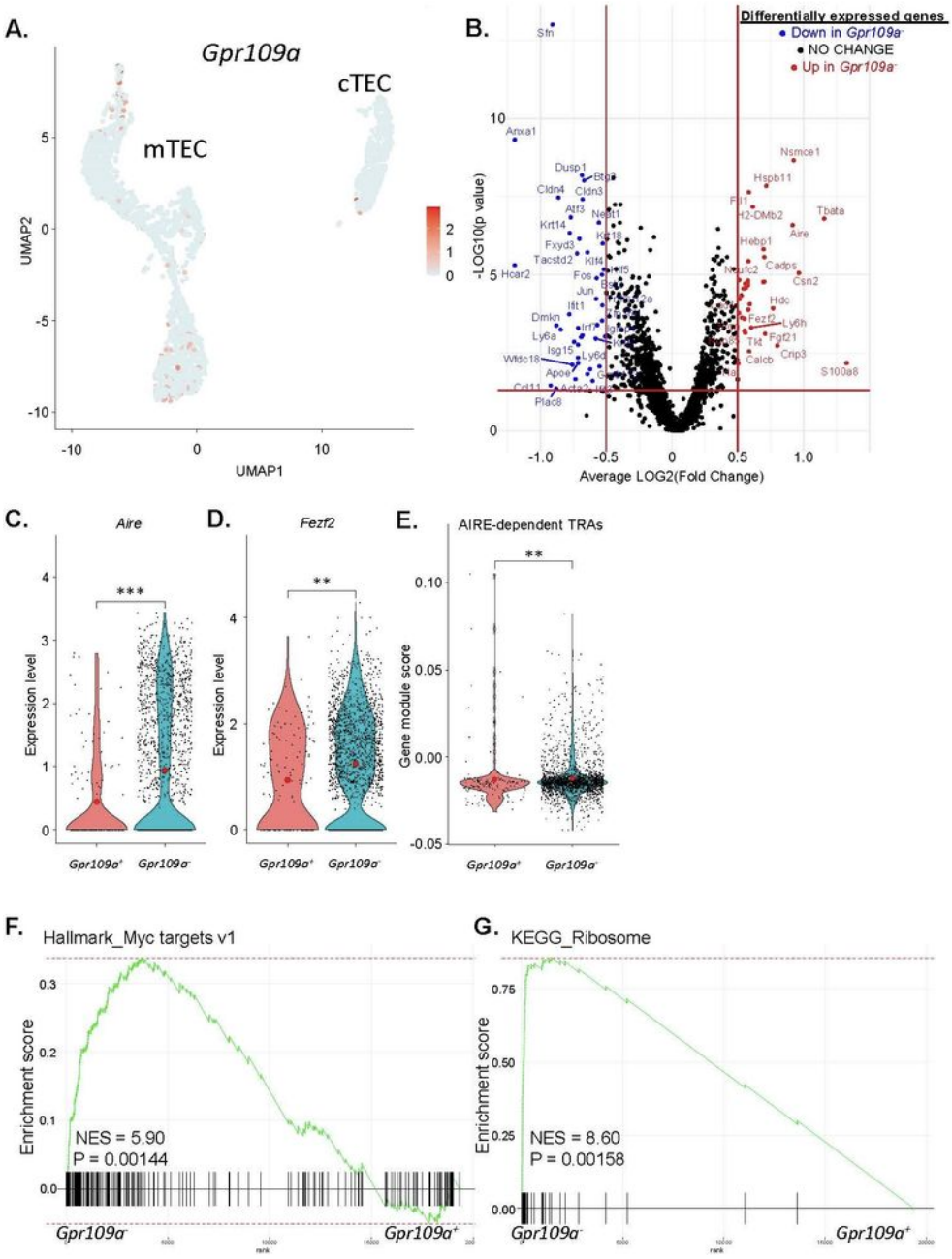

Figure 4

Single cell RNA-sequencing (scRNA-seq) of mouse thymic epithelial cells identifies Gpr109a-expressing mTEC subset, which exhibits reduced mTEC functions and re-wired intracellular signals.

A. Gpr109a is expressed predominantly in mTECs but not thymic cortical epithelial cells (cTECs). The uniform manifold approximation and projection (UMAP) visualized mouse mTECs and cTECs from

scRNA-seq results. Colored dots denoted cells that expressed Gpr109a, and the color density reflected the expression level of Gpr109a.

B. Volcano plot showing differentially expressed genes in the comparison of Gpr109a+ and Gpr109a- mTECs. The red dots denoted genes up-regulated in Gpr109a- mTECs, the blue dots denoted genes down-regulated in Gpr109a- mTECs, and the black ones are genes without significant changes.

(C-D) Violin plots of the expression profiles of Aire (C) and Fezf2 (D) in Gpr109a+ mTECs (red) versus Gpr109a- mTECs (cyan). Red dots indicate the average expression levels of the corresponding groups.

E. Violin plots of the gene module score of AIRE-dependent tissue restricted antigen (TRA) genes in Gpr109a+ mTECs (red) versus Gpr109a- mTECs (cyan). Red dots indicated the average expression levels of the corresponding groups.

(G-H) Gene set enrichment analysis (GSEA) showing enrichment of Myc-target signalling and ribosomal signalling pathways in Gpr109a+ mTECs versus Gpr109a- mTECs.

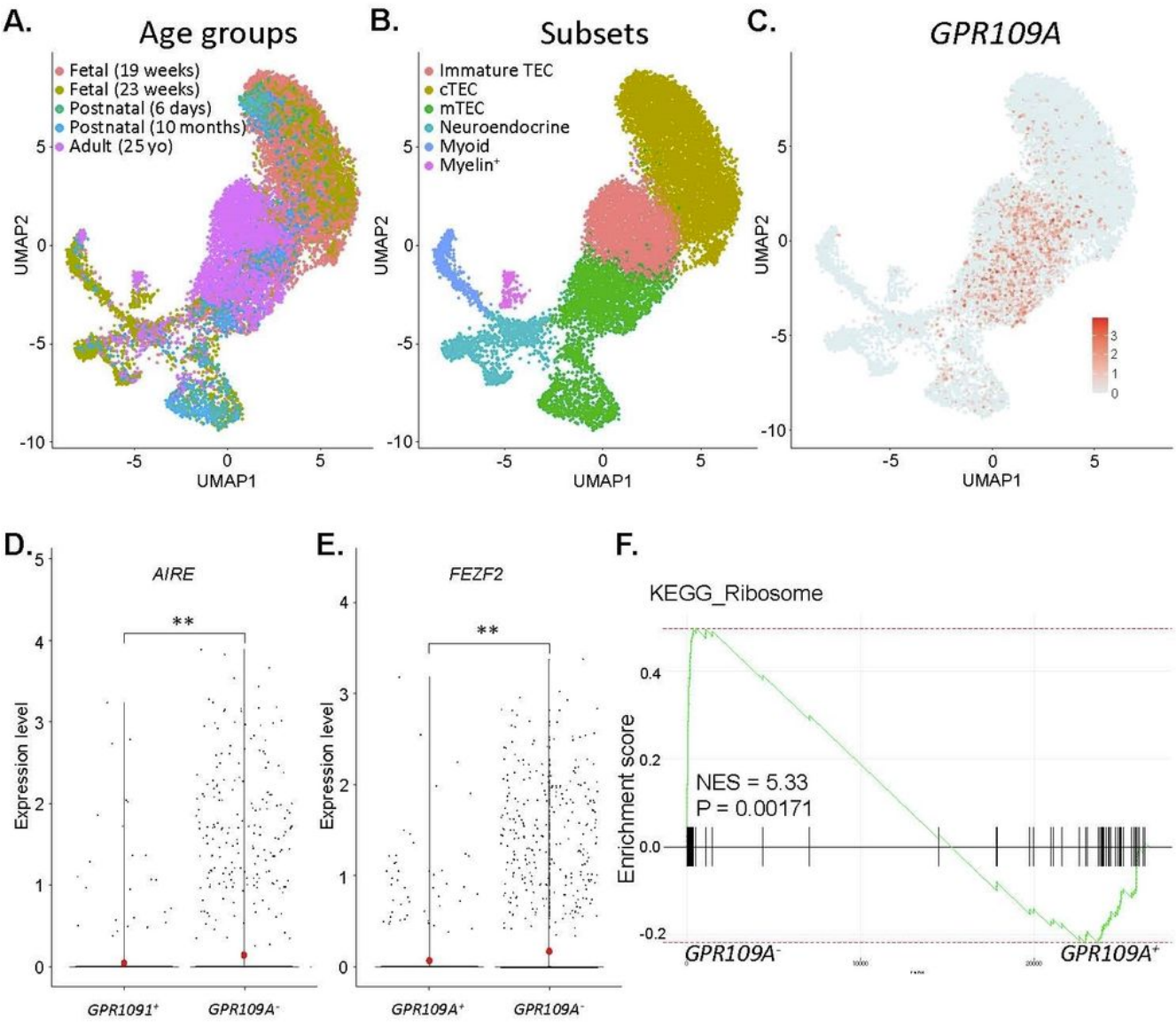

Figure 5

scRNA-seq of human thymic stroma cells identifies GPR109Aexpressing mTEC subset, which exhibits reduced mTEC functions and rewired intracellular signals.

A. The UMAP visualized thymic stromal cells colored by age group (fetal 19 weeks, fetal 23 weeks, postnatal 6 days, postnatal 10 months and adult 25 years old).

B. The UMAP visualized thymic stromal cells colored by cell types (immature TEC, cTEC, mTEC, neuroendocrine cell, myoid cell, and myelin+ cell).

C. GPR109A is expressed predominantly in mTECs and immature TECs but not cTECs. The UMAP visualizes human thymic stroma cells from scRNA-seq results. Colored dots denote cells that expressed GPR109A, and the color density reflects the expression level of GPR109A.

(D-E) Violin plots of the expression profiles of AIRE (D) and FEZF2 (E) in GPR109A+ mTECs (red) versus GPR109A- mTECs (cyan). Red dots indicate the average expression levels of the corresponding groups.

F. GSEA showing enrichment of ribosomal signalling pathways in GPR109A+ mTECs versus GPR109A- mTECs.

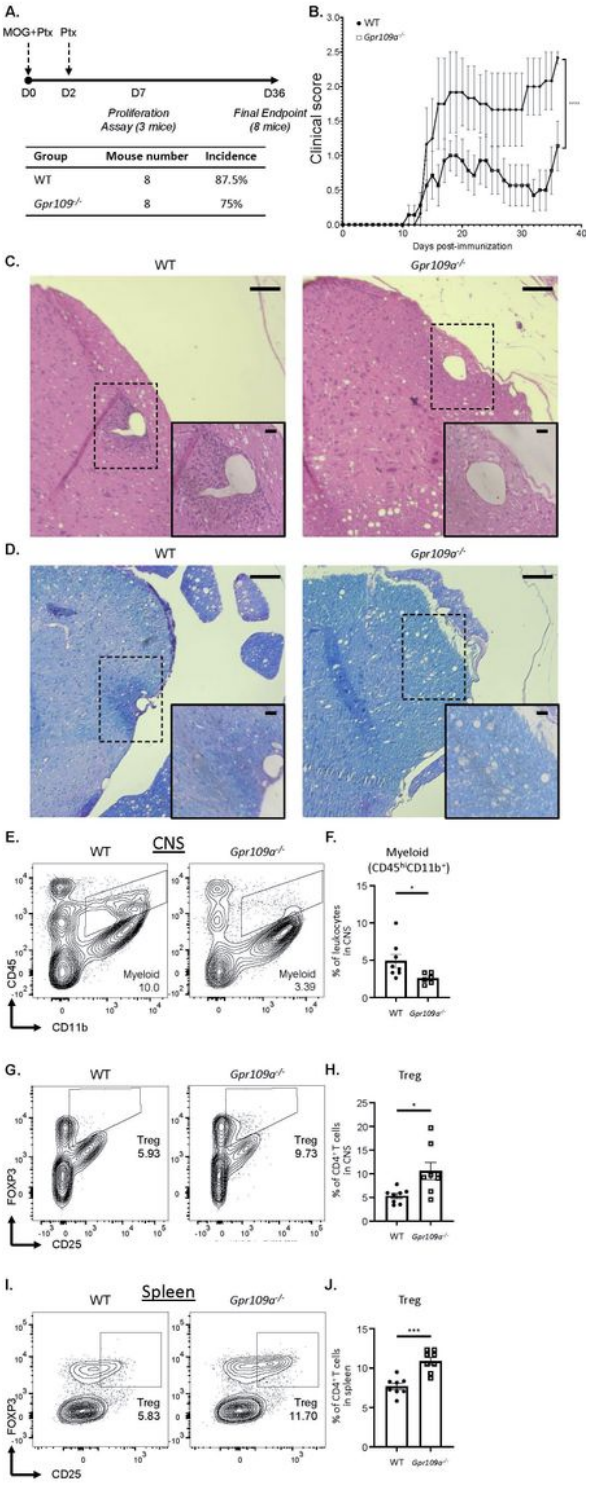

Figure 6

Gpr109a−/−mice show attenuated experimental autoimmune encephalomyelitis (EAE) compared with WT mice.

A. Study timeline. WT or Gpr109a−/− mice were immunized with myelin oligodendrocyte glycoprotein (MOG) emulsified in incomplete Freund's adjuvant supplemented with heat-killed M.Tuberculosis and

injected with pertussis toxin at D0, and 2 days later animals received second injection of pertussis toxin. On D7, 3 mice from each group were sacrificed and their draining lymph nodes were dissected and used for an ex vivo MOG-specific proliferation assay. The remaining 8 mice from each group were kept and monitored for clinical signs until culled on D36 as the final endpoint. Total mouse number for study, disease incidence and disease-related mortality are reported in the table.

B. EAE clinical course of sick mice during EAE comparing WT (filled dots) and Gpr109a−/− (hollow dots) mice (n=6-7 per group).

C. Histological analysis of spinal cord neuroinflammation of WT and Gpr109a−/− mice isolated at D30 post EAE induction with Hematoxylin and eosin (H&E) staining. Scale bar for lower resolution = 100μm, and scale bar for higher resolution = 20μm.

D. Histological analysis of spinal cord demyelination of WT and Gpr109a−/− mice isolated at D30 post EAE induction with Luxol fast blue (LFB) staining. Scale bar for lower resolution = 100μm, and scale bar for higher resolution = 20μm.

(E-F) Proportions of inflammatory myeloid cells (CD11b+ CD45hi) of the total leukocytes in CNS were analyzed by flow cytometry for WT and Gpr109a−/− mice. E. Representative flow cytometric plots of inflammatory myeloid cells in CNS from WT (left) and Gpr109a−/− (right) mice. F. Scatter bar chart for the proportions of inflammatory myeloid cells in CNS from WT and Gpr109a−/− mice.

(G-H). Proportions of Treg of the total CD4+ T cells in CNS of WT and Gpr109a−/− mice. G. Representative flow cytometric plots of Treg in CNS of WT (left) and Gpr109a−/− (right) mice. H. Scatter dot plots of the proportions of Treg in CNS from WT and Gpr109a−/− mice.

(I-J). Proportions of Treg of the total CD4+ T cells in spleens of WT and Gpr109a−/− mice. I. Representative flow cytometric plots of Treg in spleens of WT (left) and Gpr109a−/− (right) mice. J. Scatter dot plots of the proportions of Treg in spleens from WT and Gpr109a−/− mice.

N=11 per group for the overall study, but N=8 per group for the clinical course investigation and flow cytometry experiments. Data are presented as mean ± s.e.m. with * $p<0.05$, *** $p<0.001$, **** $p<0.0001$ by unpaired t-test and two-way ANOVA for the clinical curve analysis.

Supplementary Files

This is a list of supplementary files associated with this preprint. Click to download.

- Nietal.SI1.pdf